NAME OF AUTHOR.....J.J.W. BOGAARDS...............

TITLE OF THESIS.....THE $^{48}Ca(d,p)^{49}Ca$ REACTION...

....

....

UNIVERSITY...OF..ALBERTA...........................

DEGREE FOR WHICH THESIS WAS PRESENTED...Ph.D...........

YEAR THIS DEGREE GRANTED....1970.....................

Permission is hereby granted to THE NATIONAL LIBRARY

OF CANADA to microfilm this thesis and to lend or sell copies

of the film.

The author reserves other publication rights, and

neither the thesis nor extensive extracts from it may be

printed or otherwise reproduced without the author's

written permission.

(Signed)...Jn. JW Bogaards....

PERMANENT ADDRESS:

.DEPT..OF..PHYSICS.....

.LAVAL..UNIVERSITY....

..QUEBEC,..QUEBEC...

DATED..DEC..5.,.1969....19

THE UNIVERSITY OF ALBERTA

THE ^{48}Ca(d,p)^{49}Ca REACTION

by

$\copyright$ Jan Jacobus Willem Bogaards

A THESIS

SUBMITTED TO THE FACULTY OF GRADUATE STUDIES

IN PARTIAL FULFILLMENT OF THE REQUIREMENTS FOR THE DEGREE

OF DOCTOR OF PHILOSOPHY

DEPARTMENT OF PHYSICS

EDMONTON, ALBERTA

Spring, 1970

UNIVERSITY OF ALBERTA

FACULTY OF GRADUATE STUDIES

The undersigned certify that they have read, and

recommend to the Faculty of Graduate Studies for acceptance,

a thesis entitled THE ^{48}Ca(d,p)^{49}Ca REACTION submitted by

Jan Jacobus Willem Bogaards in partial fulfillment of the

requirements for the degree of Doctor of Philosophy.

_____
(Supervisor)

_____

_____

_____

_____
External Examiner

Date _DECEMBER 3, 1969_

ABSTRACT

The reactions $^{48}Ca(d,d)^{48}Ca$, $^{48}Ca(d,p)^{49}Ca(0)$ and
$^{48}Ca(d,p)^{49}Ca(2.028)$ have been studied in the deuteron energy
range 2.3 MeV to 6.0 MeV. The experimental work for each
reaction consisted of the following: (1) seven angular distri-
butions; (2) yield curves at five angles; (3) an angular distri-
bution of the analyzing power at E_d = 5.5 MeV, obtained with
polarized deuterons. The polarized deuteron work was done in
collaboration with Dr. P. Quinn and Professor W. Haeberli at the
University of Wisconsin, Madison, Wisconsin.

Average deuteron Optical Model parameters for the energy
range have been determined, and it was established from the
combined elastic scattering cross section and polarization data
that the deuteron real well depth is of the order of 100 MeV.
The spectroscopic factors of the ground state and first excited
state have been determined as 0.98 and 1.06 respectively. The
j-values of the ground state and first excited state are $3/2^-$
and $1/2^-$ as determined from the vector analyzing power for these
states. The j-dependence of the angular distributions at higher
energies has been reproduced with the DWBA calculations. The
angular distributions and yield curves predicted from the DWBA
calculations fit the data very well, particularly in the case of
the first excited state. It is concluded that the DWBA theory
represents the direct reaction process well.

ACKNOWLEDGEMENTS

TABLE OF CONTENTS

LIST OF TABLES

LIST OF FIGURES

CHAPTER 1

INTRODUCTION

Deuteron stripping experiments are generally performed
at energies above the Coulomb barrier where the distinctive
features of the angular distributions allow the extraction
of nuclear structure information, particularly the 1-value
of the absorbed particle. At energies below the Coulomb
barrier, however, the angular distributions lose their
distinctive features and are almost independent of the trans-
ferred 1-value (Ma 64, Ma 64a) so that this information can not
be extracted. Because of the presumed paucity of the infor-
mation that can be obtained at sub-Coulomb energies, this
energy region has been somewhat neglected by experimentalists.
This situation is rather unfortunate since it implies that
low energy facilities, such as Van de Graafs, can not be used
for stripping experiments on heavy nuclei which have high
Coulomb barriers.

It has been pointed out recently, however, that sub-
Coulomb stripping may be useful in the determination of reduced
widths and spectroscopic factors (Go 65, Gi 66). In addition,
it has been shown that 1-values of the transferred particle
may be determined from the slope of the yield curve at

backward angles at energies below and slightly above the

Coulomb barrier (He 68). The reliability and accuracy of

the information that may be obtained depends on the validity

of the interaction theory, the Distorted Wave Born Approximation

(DWBA) theory, that is used in the analysis. Extensive studies

of the validity of the DWBA theory have been made at higher

energies (Le 64, Se 69) but at present no study has been done

connecting sub-Coulomb stripping with higher energy stripping.

It was felt, therefore, that it would be of interest to

perform a study which would encompass both energy regions so

that the continuity of the data would provide a link between

the energy regions.

The reactions $^{48}Ca(d,p)^{49}Ca(0)$ and $^{48}Ca(d,p)^{49}Ca(2.028)$

were chosen for this study for several reasons. First, ^{48}Ca

is a closed shell nucleus (20 protons and 28 neutrons) so that

the final states in ^{49}Ca are expected to be good single-particle

states, i.e., the states correspond to the addition of a single

neutron to an inert and spherical core (Be 68, An 68). Since

the spectroscopic factor is therefore expected to be unity,

the ability of DWBA to give absolute cross sections can be

tested critically. The energy level diagram of ^{49}Ca is shown

in Fig. 1.1.

Secondly, Hauser-Feshbach calculations indicate that

the compound nucleus contributions are small, particularly in

the case of the $^{49}Ca(2.028)$ state.

Figure 1.1   Energy level diagram of ^{49}Ca (from Ka 64).
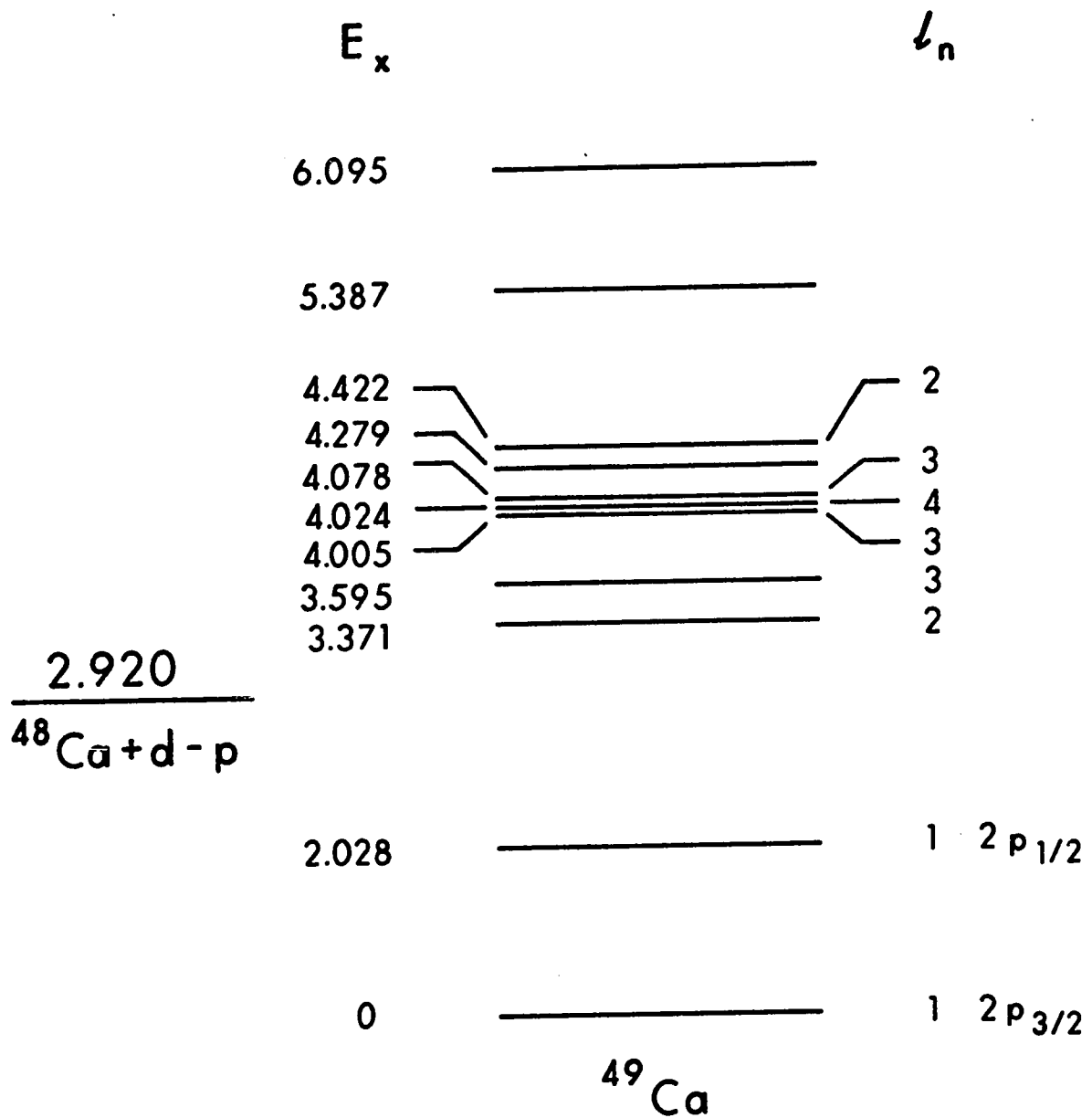
Thirdly, the two energy regions, which involve three possible energy combinations of the incoming and outgoing particles can be covered within the energy range of the University of Alberta Van de Graaff accelerator for ^{48}Ca, since ^{48}Ca has a Coulomb barrier of about 4.75 MeV and a ground state Q-value for the (d,p) reaction of 2.92 MeV. The three energy combinations are listed below; the first column shows the energy combination, the second column the deuteron energy range for which this combination holds, and the third column the state of ^{49}Ca that is involved (E_d denotes the incident deuteron energy, E_p the outgoing proton energy and E_c the Coulomb barrier energy).

(1) $E_d > E_c$, $E_p > E_c$ $E_d > 4.75$ MeV ^{49}Ca(0)
                                                          ^{49}Ca(2.028)

(2) $E_d < E_c$, $E_p > E_c$ 2.0 MeV $< E_d < 4.75$ MeV ^{49}Ca(0)
                                   4.0 MeV $< E_d < 4.75$ MeV ^{49}Ca(2.028)

(3) $E_d < E_c$, $E_p < E_c$ $E_d < 2.0$ MeV ^{49}Ca(0)
                                   $E_d < 4.0$ MeV ^{49}Ca(2.028)

The experimental work for this study consists of the following:

1)   seven angular distributions of the (d,d) and (d,p) reactions, obtained simultaneously, for deuteron energies between 2.5 MeV and 5.5 MeV;

2) yield curves of the (d,d) and (d,p) reactions at

    five angles (65°, 90°, 115°, 145° and 165°) over a

    deuteron energy range of 2.3 MeV to 6.0 MeV, the

    upper part of the range in 10 KeV steps, the lower

    part mostly in 20 KeV steps;

3) the angular distributions of the analyzing power of

    the (d,d) and (d,p) reactions, obtained with vector

    polarized deuterons at the University of Wisconsin,

    Madison, Wisconsin, in collaboration with Dr. P.

    Quinn and Professor W. Haeberli.

A short description of each of the following chapters
will be given here. A descriptive account of the Optical Model
and DWBA theory is given in Chapter 2. The experimental method
and data reduction are described in Chapter 3. The Optical
Model analysis as well as the DWBA calculations are presented
in Chapter 4. Chapter 5 contains a summary of the results and
conclusions. Differential cross sections and the analyzing
power for the angular distributions are listed in Appendix A.

CHAPTER 2

THEORY

2.1 The Optical Model

The scattering of a projectile, such as a deuteron,
from a target nucleus should ideally be described in terms
of the two-body forces that exist between the nucleons in
the projectile and the nucleus. Unfortunately, this
approach is too complex in most cases and it is therefore
necessary to use an approximation. In this approximation,
known as the Optical Model, the nucleus is replaced by an
average potential so that the many-body problem is reduced
to a two-body problem.

The form of the optical potential employed in this
work is

$$U(r) = V_c(r) - Vf(x_o) + 4i \, W \frac{d}{dx_i} f(x_i)$$

$$[\frac{\hbar}{m_\pi c}]^2 \frac{V_{SO}}{r} \frac{d}{dr} f(x_{SO}) \, \vec{L}.\vec{\sigma}$$

2.1

In Eq. 2.1 $V_c(r)$ is the Coulomb potential of a uniformly
charged sphere with

$$V_c(r) = \frac{Zze^2}{2R_c} \; [3 - (\frac{r}{R_c})^2] \qquad\qquad r \leq R_c = r_c A^{\frac{1}{3}}$$

$$V_c(r) = \frac{Zze^2}{r} \qquad\qquad\qquad\qquad r \geq R_c$$

The shapes of the nuclear potential wells are determined by

$$f(x) = (1 + e^x)^{-1}, \qquad\qquad 2.2$$

the Woods-Saxon form factor, where

$$x_o = \frac{r - r_o A^{\frac{1}{3}}}{a_o} \qquad\qquad x_i = \frac{r - r_i A^{\frac{1}{3}}}{a_i}$$

$$\qquad\qquad 2.3$$

$$x_{SO} = \frac{r - r_{SO} A^{\frac{1}{3}}}{a_{SO}}$$

The parameters r_o, r_i and r_{SO} will be referred to as the real, imaginary and spin-orbit radius respectively; the parameters a_o, a_i and a_{SO} will be referred to as the real, imaginary and spin-orbit diffuseness. The depths (or strengths) of the potentials are determined by V, the real well depth, W, the imaginary well depth, and V_{SO}, the spin-orbit well depth. The real and imaginary potentials will be referred to as the central potentials. The shapes of the three potentials as well as the real part of the radial wavefunction for an $\ell=0$ incident deuteron (a part

of the solution to the Schroedinger equation) are shown
in Fig. 2.1.

The three potentials are necessary elements of the
overall optical model potential in order to explain the
scattering, absorption and polarization of incident
particles. The real potential V is refractive, i.e., the
wavelength of the incident particle is changed but the
total flux of the particles is unaltered. Although the
Woods-Saxon form of this potential is a mathematical
compromise, in that it is relatively simple to handle, it
does reflect the basic nuclear properties. It is nearly
constant close to the centre of the nucleus, thus reflecting
the saturation properties of the nuclear forces. It also
has a diffuse surface, a feature of the potential which
was found necessary early in the development of the optical
model (Ja 55, Ne 55), since the diffuseness affects the
number of particles reflected or absorbed at the surface
(Vo 62, Em 63).

The imaginary potential W is absorptive. Particles
are thus removed from the incident beam to form a compound
nucleus, produce inelastic reactions, etc. The argument
that the Pauli exclusion principle prevents collisions,
particularly in the dense nuclear interior and at low
energies, leads to the conclusion that the imaginary

Figure 2.1   Shapes of the real, imaginary and spin-

orbit potentials, labelled V, W and V_{SO}

respectively. The curve labelled

"incident deuteron" shows the real part

of the radial wavefunction for an $\ell=0$

deuteron incident on the shown potentials.
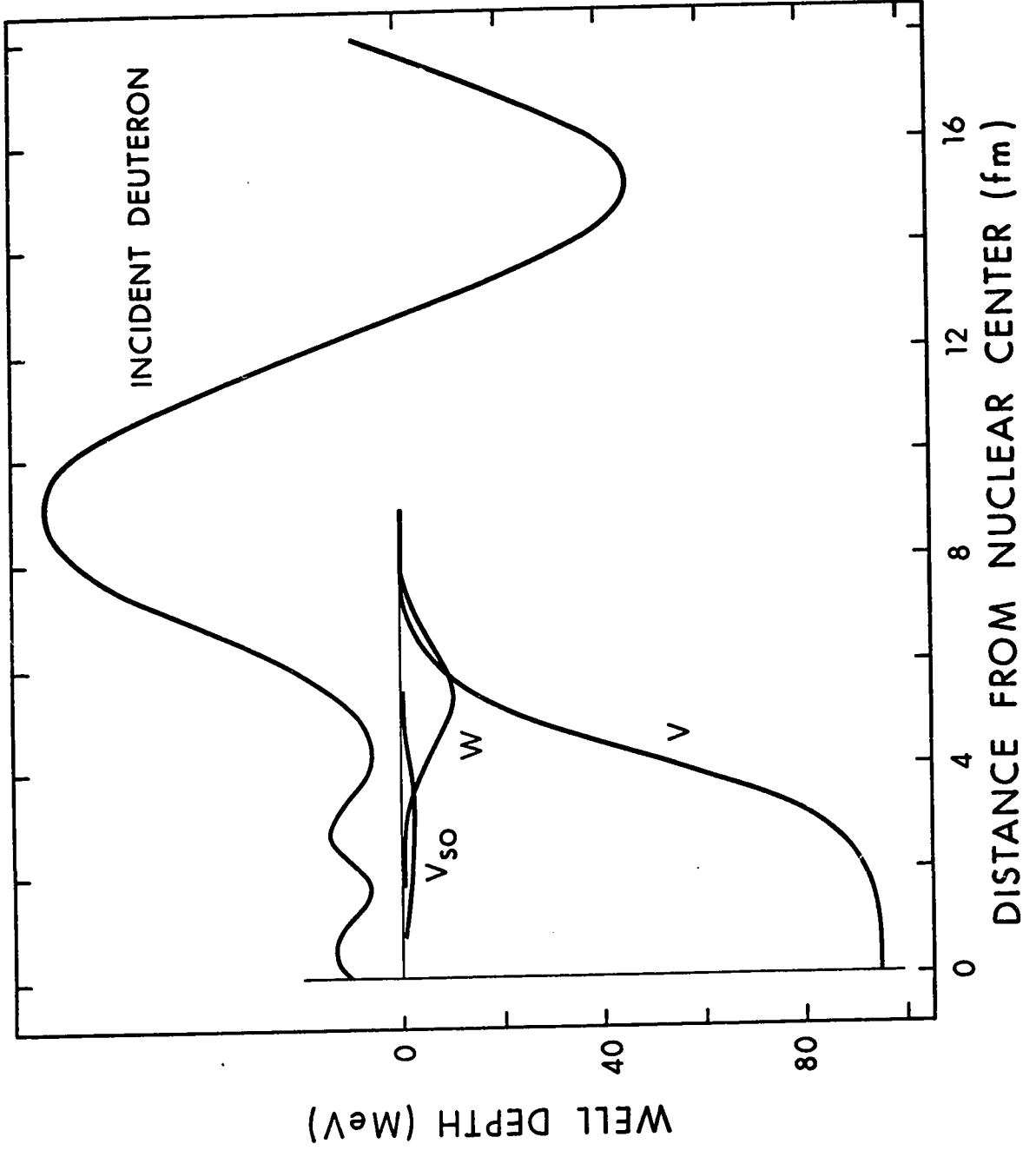
potential should be strongest in the surface region. Early attempts to concentrate the imaginary potential in the surface region failed to give the correct angular distributions when a square well potential was used. It was found, however, that the introduction of a real well diffuseness allowed the placement of the imaginary well near the surface (Em 63). In order to obtain the surface peaked imaginary potential, the derivative of the Wood-Saxon form factor is used (See Eq. 2.1 and Fig. 2.1).

The spin-orbit potential has the customarily employed Thomas form (Bl 55, Bj 58). The theoretical justification of this form (Gr 68) is not clear cut, since the exact origin of this force is not known. The fact that its radial dependence is peaked at the surface is considered reasonable on the grounds that the particles of high angular momentum, which are known to experience the largest spin-orbit splitting, spend most of their time at the surface of the nucleus (Wa 68). Although the strength of the spin-orbit potential is small compared to the real potential strength, it is a necessary part of the total potential since it affects different spin states to a different extent and thus produces polarization of the scattered particle.

There is evidence (Pe 62, Pe 63) that the nuclear potentials are non-local. The potential should therefore

not be a function of a single coordinate $\vec{r}$ but rather
should reflect the fact that the presence of a particle
at $\vec{r}$ influences the probability of finding the particle
at the position $\vec{r}'$ in the neighbourhood of $\vec{r}$. An effective
potential V, dependent only on $\vec{r}$, can be expressed as an
integral operator of the form (Pe 62)

$$V\Psi = \int U(\vec{r},\vec{r}')\Psi(\vec{r}')d^3\vec{r}' \qquad 2.4$$

and as such V is energy dependent.

Since the true non-local potential is too complex
to handle, the local energy approximation is made. In this
approximation the wavefunction is multiplied by a constant
depending on the well depth and the range of the non-locality
(Hj 65). This relatively simple approach appears to be a
good approximation (Ul 68), particularly so since it reduces
the amplitude of the elastic scattering wave (Le 64), which
simulates part of the effect of the exclusion principle.

The well depth, the radius and the diffuseness of
each of the three potentials are normally determined with a
computer search program. In such a program one or more
parameters will be searched while the other parameters
remain fixed. The program then determines the best value
for each searched parameter on the basis of a comparison
between the calculated and the experimental angular
distribution through the goodness-of-fit parameter χ^2,

$$\chi^2 = \sum_{i=1}^{N} \left[\frac{Q_{calc}(\theta_i) - Q_{exp}(\theta_i)}{\Delta Q(\theta_i)}\right]^2 \qquad 2.5$$

where

N is the number of data points in the experimental angular distribution

$Q_{exp}(\theta_i)$ is the experimentally determined quantity, e.g., the differential cross section, at angle θ_i

$Q_{calc}(\theta_i)$ is the quantity at θ_i calculated from the optical model parameters

$\Delta Q(\theta_i)$ is the experimental error at θ_i

In the case of the proton the optical model parameters are now reasonably well determined (Ro 66, Vo 68, Be 69), in particular, the real well depth which in this case is about 52 MeV. In the case of the deuteron the situation is not as clear. It is generally argued that the real well depth for the deuteron should be approximately the sum of the well depths for the proton and the neutron, i.e., of the order of 100 MeV, a figure that is corroborated by the calculations of Perey and Satchler (Pe 67). It is hoped, however, that an extensive study of deuteron elastic scattering data, similar to the study done lately by Becchetti and Greenlees (Be 69) may improve the situation.

Mention should be made of the ambiguities that exist

in the parameters, for example the Vr_o^n ambiguity. Where

such ambiguities exist it is found that an increase in one

parameter accompanied by the appropriate decrease in the

associated parameter will produce an equally acceptable

fit to the experimental data and thus presumably an equally

acceptable set of parameters. In some cases a set of

parameters can be rejected on the basis that some parameters

are "unphysical," for instance when the parameter set

contains a real radius of 0.2 fm. In many cases, however.

the situation is not as clear and it is then, if possible,

necessary to determine the optimum set of parameters from

criteria outside the fitting procedure.

2.2 The Distorted Wave Born Approximation

The Distorted Wave Born Approximation (which will be

referred to as DWBA) is a particular approach to the type

of nuclear reactions known as direct reactions. In a direct

reaction the transition from the incident channel (initial

state) to the reaction channel (final state) in a nuclear

reaction is considered to take place in one step without

the formation of an intermediate state. The DWBA theory

of nuclear reactions can be seen as an extension of the

previously described optical model since DWBA takes the

optical model as a first approximation but introduces as a perturbation an additional interaction which gives rise to non-elastic processes.

Since a direct reaction is considered as a perturbation, the transition amplitude T, and thus the differential cross section $(d\sigma/d\Omega) \propto T^2$, can be derived from perturbation theory. Thus, if a reaction proceeds from an initial state Ψ_i to a final state Ψ_f through the action of the perturbing potential V', the transition amplitude T is given by

$$T = \int \Psi_f V' \Psi_i d\tau \qquad\qquad 2.6$$

The perturbing potential V' can be determined from a comparison of the total Hamiltonian H_t for the system with the Hamiltonian H_f of which the final state is an eigenfunction. In order to determine this potential, consider the deuteron stripping reaction A(d,p)B where

A	is the target nucleus
d	is the incident deuteron
B	is the residual or final nucleus consisting of the target nucleus A plus the transferred neutron n
p	is the emerging proton

The total Hamiltonian H_t for this system can be written as

$$H_t = T_{dA} + T_{pn} + V_{pn} + V_{pA} + V_{nA}$$
$$= T_{nA} + T_{pB} + V_{pn} + V_{nA} + V_{pA} \qquad 2.7$$

where

T_{dA} is the operator for the relative kinetic

energy of the deuteron-target system

V_{pA} is the potential energy of the proton-

target system, and so on.

The final state wave function is an eigenfunction of

the Hamiltonian H_f

$$H_f = T_{nA} + T_{pB} + V_{nA} + \overline{V}_{pB} \qquad 2.8$$

where $\overline{V}_{pB}$ is not the true potential acting between the proton

and the residual nucleus B but the simpler optical model

potential as determined from the elastic scattering of protons

from nucleus B. A comparison of Eq. 2.8 with the last part of

Eq. 2.7 shows that the perturbing potential V' is given by

$$V' = H_t - H_f = V_{pn} + V_{pA} - \overline{V}_{pB}$$

The contribution of $V_{pA} - \overline{V}_{pB}$ to the integral in Eq. 2.6

is difficult to evaluate or to simplify (To 61) and it is

usually argued that there must be considerable cancellation

between V_{pA} and $\overline{V}_{pB}$ although this cancellation can never be

complete for finite nuclei, particularly since V_{pA} allows the

nucleus to be excited (Le 64). If these terms are dropped,

however, the effective perturbing potential V' becomes simply

$$V' = V_{pn} \qquad 2.9$$

Equation 2.6 can now be written more explicitly as

$$T = \int\int \chi_p^{(-)}(\vec{k}_p, \vec{r}_p)^* <B|V_{pn}|A> \chi_d^{(+)}(\vec{k}_d, \vec{r}_d) d\vec{r}_p d\vec{r}_d \qquad 2.10$$

where χ_d and χ_p are the incoming deuteron and outgoing proton distorted waves respectively. The distorted waves are generated from the optical model potentials which have been determined from the elastic scattering of the deuteron from nucleus A and the proton from nucleus B. In many cases the residual nucleus B is unstable so that no elastic scattering measurements can be made to determine the proton optical model parameters directly. In these cases the proton optical parameters that belong to the scattering of protons from nucleus A or some neighbouring nucleus are used.

The term in brackets in Eq. 2.10 is the matrix element of the interaction integrated over all coordinates independent of r_d and r_p (Sa 60, Ro 61). Thus essentially all the physics of the interaction appears in this factor which may be written as

$$\phi_n V_{pn} \phi_d \qquad 2.11$$

where ϕ_n describes the transferred neutron bound to the target nucleus, a shell model wave function, and ϕ_d is the internal wave function of the deuteron.

Because relatively little is known about the potential V_{pn} and because of the complexity of the integral in Eq. 2.10 an approximation has to be made in Eq. 2.11. In this approximation,

the range of V_{pn} is set to zero. The product $V_{pn}\phi_d$ can then be expressed (To 61, Ba 62) as the product of a constant factor and a delta function. Inherent in this approximation is the restriction that in the reaction the proton appears exactly where the deuteron disappeared. This is a rather unsatisfactory restriction since the deuteron is a large, diffuse particle (Bl 62). A correction factor that simulates the effect of the finite size of the deuteron (the finite range correction (Bu 64)) is therefore applied to the form factor.

Although the DWBA theory is an oversimplification of the true reaction theory, it has been an extremely useful tool for many years in nuclear spectroscopy, particularly in the determination of the 1-value of the transferred nucleon (Be 65, Fi 68). It appears now that the DWBA theory will also be able to determine j-values (Yu 68, Se 69) so that additional information can be obtained. But beyond the usefulness of DWBA as a spectroscopic tool lies the expectation that a determination of the limits of the validity of this interaction model will provide insight into the true nature of nuclear reactions.

CHAPTER 3

EXPERIMENTAL WORK AND DATA REDUCTION

3.1 Target Preparation

The natural abundance of ^{48}Ca is 0.18% and it was therefore necessary to use enriched target material. The target material, in the chemical form of $CaCO_3$, was obtained from Oak Ridge National Laboratory.

When $CaCo_3$ is heated, CO_2 is driven off, leaving CaO as the material to be evaporated. CaO has a melting point of about 2600°C, a temperature that cannot be reached in a standard heated boat evaporator. Several authors (Ma 66, Be 68), however, have reported the preparation of Ca targets, starting from $CaCO_3$, with the use of a heated Ta boat. Trial evaporations were therefore made with standard $CaCO_3$ in a Ta boat. These trial evaporations showed four important points:

1) The escaping CO_2 caused the target material to "jump" and spill out of the boat.

2) Ca, not CaO was evaporated, as evidenced by the shiny appearance of the evaporated material and it's violent reaction with water.

3) The temperature at which all CO_2 was removed was substantially lower than the temperature at which the Ca was evaporated.

4) The Ta boat corroded during the evaporation

process.

It was point 4) that was of particular interest since it

indicated that Ta acted as a reducing agent for CaO, thus

producing free Ca. Since the reduction process takes place

at a substantially higher temperature ($\sim$1700°C (Ma 66))

than the melting point of Ca ($\sim$850°C), the Ca is evaporated

as soon as reduction has taken place. A series of quantitative

measurements, consisting of weighings before and after evapo-

ration, verified the observation that Ta acts as a reducer for

CaO.

In order to facilitate reduction, finely ground Ta

powder was thoroughly mixed with the $CaCO_3$ in subsequent

evaporations. The Ta powder also served the important purpose

of reducing the "jumping" of the $CaCO_3$ when the CO_2 is removed.

This jumping can cause specks of $CaCO_3$ to land on the target

backings, thus causing non-uniformities in the target.

The procedure adopted for final target preparation was

as follows (all currents quoted pertain to a boat made of 0.002"

thick Ta, 1" long, 1/2" wide):

1) Ta powder (mesh #325) was thoroughly mixed with

$CaCO_3$ in the ratio 4:1 by weight. Target blanks

with very thin Formvar on carbon backings (the Formvar

to be floated and picked up first, then the carbon)

were suspended 3 3/4"-4" above the boat, the
Formvar side facing the boat.

2) After evacuation of the bell jar, the current
through the boat was slowly raised to 25 - 28 A
at which point the outgassing of the CO_2 started.
While the pressure was monitored and not allowed
to go over 3 - 5 times base pressure (to avoid
"jumping"), the current was slowly raised until
final outgassing had occurred at 55 A.

3) The current was then quickly raised to 85 A
(this current is about 10% higher than the minimum
current at which Ca evaporates, as established in
trial evaporations). After 10 seconds the current
was lowered to 40 A for one minute, then raised
again to 85 A for 10 seconds. A total of four or
five 10 second "flashes" were usually made.

4) The targets were allowed to cool for about one hour
(under vacuum) and were then quickly transferred to
the scattering chamber.

Several comments regarding target preparation and handling should
be made. First, it is imperative that the Ca be evaporated onto
the Formvar since it was found that if the Ca is evaporated
onto the carbon, the target will start disintegrating as soon
as it is exposed to air. The carbon backing is necessary,

however, to provide a conducting layer for the target.

Because of the great expense of the target material, it would be preferable to reduce the distance between boat and target backings to increase efficiency. The distance of about 4", however, was found to be the optimum distance for target uniformity and target survival (the target backings will break when exposed to the hot boat). At this distance very uniform targets were produced with a survival rate of 60 - 90%. It should be noted that if the flash technique is not used, the survival rate is decreased by a factor of two. With the use of the above technique, targets with a thickness of 15 - 20 $\mu g/cm^2$ of ^{48}Ca were produced from 10 mg of ^{48}Ca.

Initially attempts were made to keep the ^{48}Ca from oxidizing during the transfer from the evaporator to the target chamber. It was found, however, that even the shortest contact with air caused virtually complete oxidation because of the extreme thinness of the target. These attempts were therefore abandoned. As a comforting circumstance it was found that the oxidized targets could be successfully stored for long periods of time (several months) in a glass jar that contained some drying agent. For example, one target was used after eight months of storage.

The great difficulties encountered in the evaporations and the necessity for the development of the rather elaborate

evaporation procedure were due to the requirement that very thin, and therefore very fragile, target backings be used, since low (2.5 MeV) deuteron energy runs were planned. If substantially thicker backings can be used, many of the difficulties are greatly reduced and the evaporation efficiency can be greatly increased through a reduction of the boat to backing distance. It was found, however, that target uniformity was greatly affected by such a reduction.

It is of some interest to note that Ta was also found to reduce such oxides as SiO_2, MgO and BaO at temperatures well within the range of standard evaporators. It would thus appear that the use of Ta boats and powder provides the possibility of target preparation from the oxides of elements.

3.2 Data Acquisition

The data obtained for this thesis can be divided into three parts:

(a) The angular distributions of the $^{48}Ca(d,d)^{48}Ca$, $^{48}Ca(d,p)^{49}Ca(0)$ and $^{48}Ca(d,p)^{49}Ca(2.028)$ reactions

(b) The yield curves of the (d,d) and (d,p) reactions

(c) The angular distributions of the analyzing power of the (d,d) and (d,p) reactions.

Parts (a) and (b) were obtained with the University of Alberta
Van de Graaff accelerator; Part (c) was obtained with the
University of Wisconsin, Madison, tandem Van de Graaff
accelerator.

(a) Angular Distributions

The angular distributions were taken in a scattering
chamber designed by Dr. G. Roy of the Nuclear Research Centre,
University of Alberta. A complete description of the
scattering chamber and associated equipment is given in Hu 69.
Four moveable detectors, set 10° apart at a distance of 8"
from the centre of the chamber, were used simultaneously to
obtain the angular distributions. Collimators with a circular
aperture were used with the detectors, each of the two forward
detectors subtending a solid angle of about 2×10^{-4} steradians,
each of the other two a solid angle of about 3.2×10^{-4}
steradians. Each detector was connected through a pre-amplifier
and amplifier to its own ADC. Each ADC was connected to a clock
for dead time measurements. The output of the four ADC's was
stored in the memory of the on-line SDS-920 computer (see
Fig. 3.1).

A fifth detector, subtending a solid angle of about
3.9×10^{-4} steradians and held stationary at 90° was used as a
monitor detector. It was connected to an ADC which employs its
own memory. The contents of this memory can be dumped into the
computer memory. At the end of each run the data from all five

Figure 3.1   Drawing (schematic) of the experimental

arrangement at the University of Alberta.

BEAM DEFINING SLITS

ANTI-SCATTER SLIT

TARGET CHAMBER

MONITOR COUNTER

TARGET

COUNTERS

FARADAY CUP
WITH SUPPRESSOR

PRE-AMPLIFIER

AMPLIFIER

ADC

COMPUTER
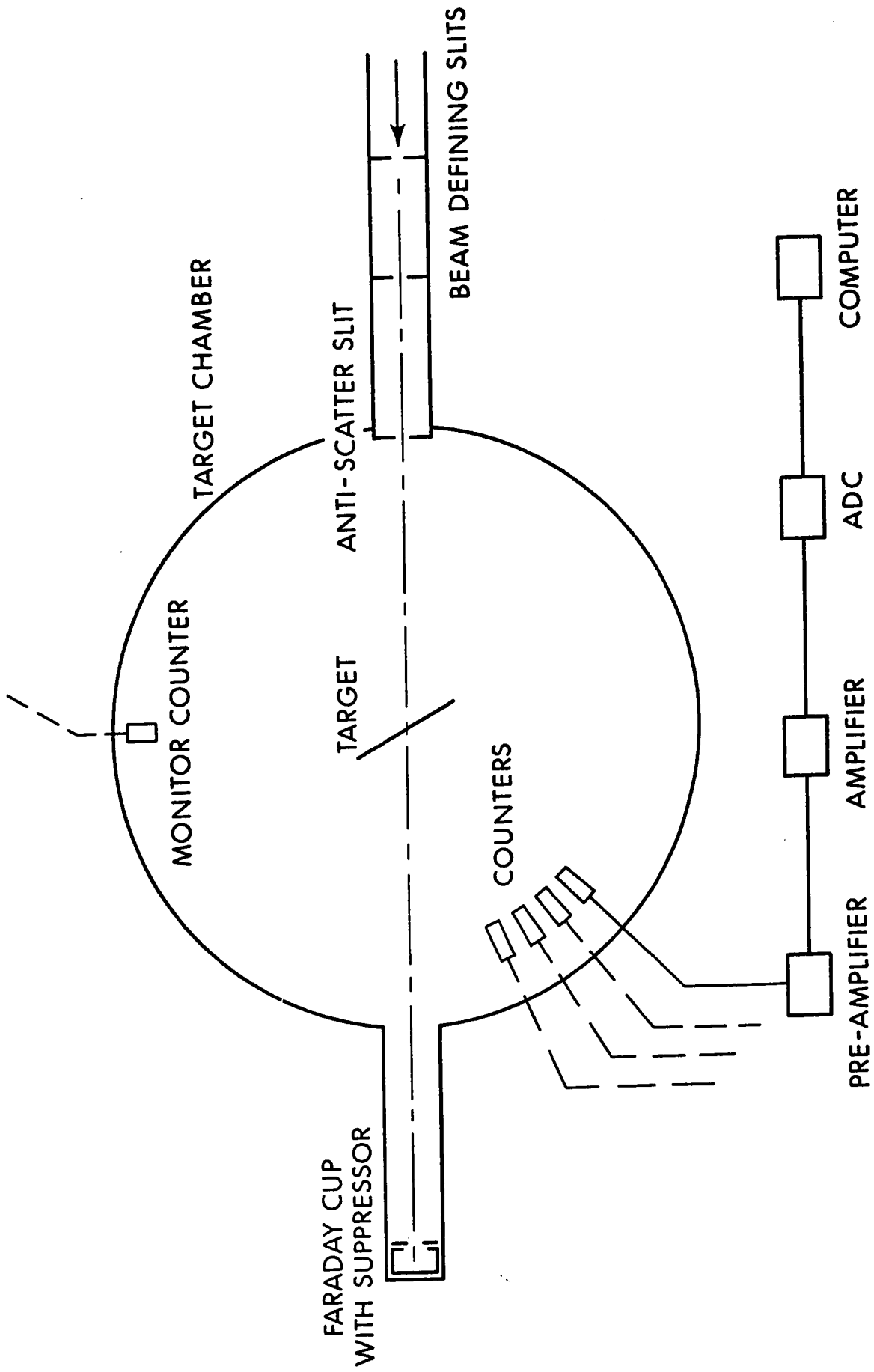
detectors was written on magnetic tape.

Charge was collected in a Faraday cup which was mounted 18" beyond the target chamber. The Faraday cup was equipped with a secondary electron suppressor biased to -1000 V and mounted slightly in front of the cup.

The composition of the Ca target employed for the angular distributions is as follows (as supplied by Oak Ridge National Laboratory):

^{48}Ca   81.9 ±0.2%

^{46}Ca   <0.05%

^{44}Ca   2.02 ±0.05%

^{42}Ca   0.31 ±0.05%

^{40}Ca   15.67 ±0.2%

traces of other elements

The target had a thickness of 15 - 20 $\mu g/cm^2$

Angular distributions were taken at incident deuteron energies of 2.5, 3.0, 3.5, 4.0, 4.5, 5.0 and 5.5 MeV, at the higher energies in 5° steps, at the lower energies in 10° steps. In addition, a partial angular distribution at forward angles was taken with 2 MeV protons to provide absolute cross sections. The detectors were cooled with liquid nitrogen and the resolution obtained was nominally 18 - 25 KeV. A typical spectrum is shown in Fig. 3.2. Dead time for any

Figure 3.2   Charged particle spectrum. The target
consisted of a layer of Ca, enriched to
81.9% in ^{48}Ca, on a thin Formvar and
carbon backing.

CHARGED PARTICLE SPECTRUM
E_d = 4.5 MeV 135°
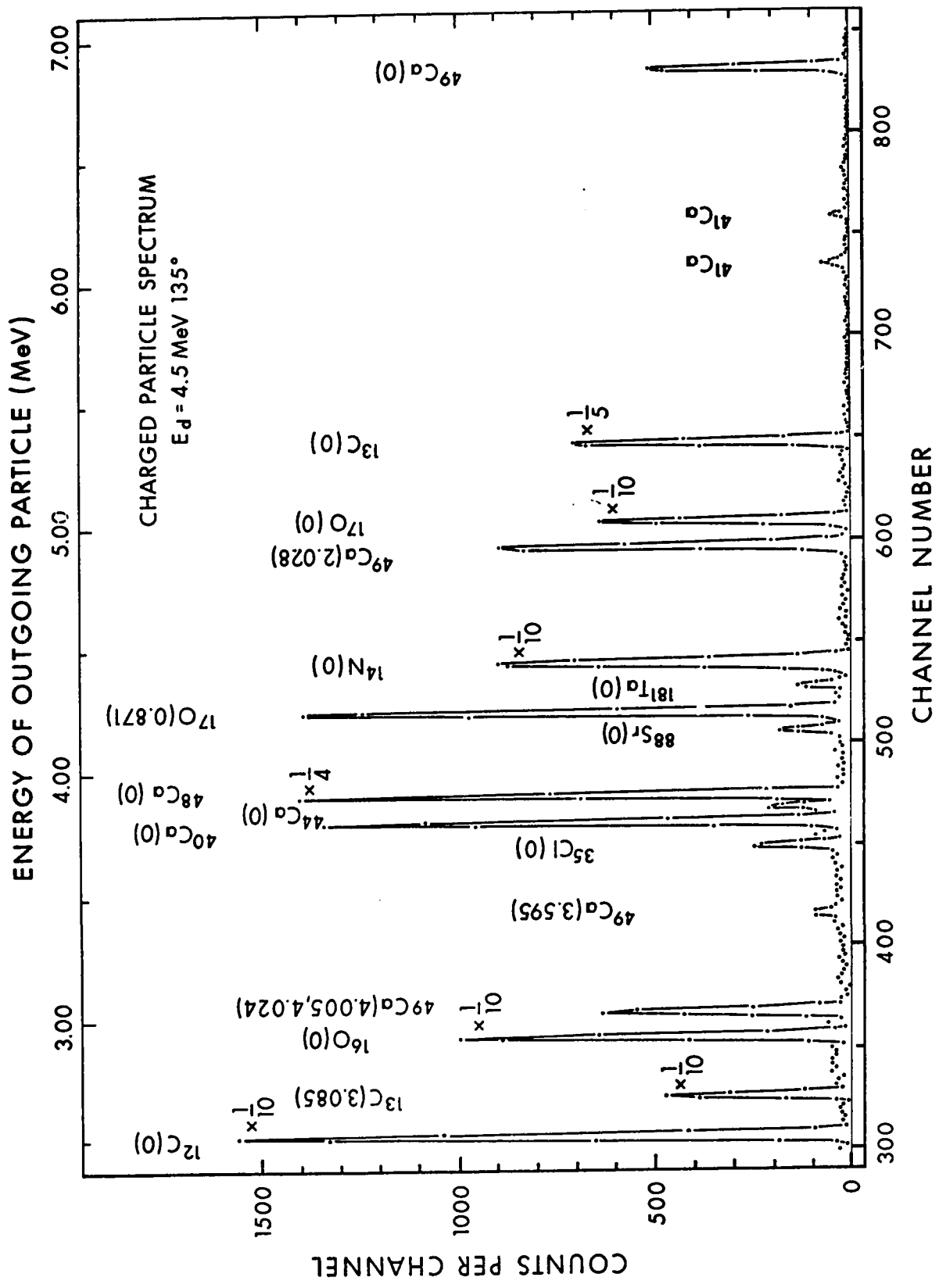
one detector was kept to less than 5%. Angles forward of
95° were taken with the target in the transmission mode
(the target at -35° to the incident beam); angles back of 85°
were taken in the reflection mode (the target at +35° to the
incident beam). It should be mentioned that previous to
the taking of the angular distributions the adjustable beam
slits (Ro 69) had been adjusted such that a minimum number
of background counts were detected when a target blank was
used instead of a complete target.

In order to gain self-consistency of the data, the
following procedure was adopted. Data was taken in the
reflection mode at the first deuteron energy (4.5 MeV), then
in the transmission mode. Without a change in the target
position, data was taken at the next energy in the transmission
mode, then in the reflection mode, and so on. The 2 MeV proton
data was included in this procedure. At each energy the
monitor counter provided the normalization constant between
the two target modes, if needed.

It should be noted that at each energy several angles
were repeated as checks. In addition, angles were repeated
at previously run energies to detect target deterioration.

(b) Yield Curves

The experimental arrangement for the yield curves was
the same as the one employed for the angular distributions.

The five detectors were positioned at 65°, 90°, 115°, 145° and 165°. The energy range between 2.3 MeV and 6.0 MeV was covered as follows:

$$2.30 - 2.50 \text{ MeV} \quad \text{in} \quad 50 \text{ KeV steps}$$

$$2.50 - 2.70 \text{ MeV} \quad \text{in} \quad 40 \text{ KeV steps}$$

$$2.70 - 3.75 \text{ MeV} \quad \text{in} \quad 20 \text{ KeV steps}$$

$$3.75 - 6.00 \text{ MeV} \quad \text{in} \quad 10 \text{ KeV steps}$$

A target of 15 - 20 $\mu g/cm^2$ was used; the composition of the target (as supplied by Oak Ridge National Laboratory) is given below:

^{48}Ca 97.16 ±0.05%

^{46}Ca <0.02

^{44}Ca 0.10 ±0.02%

^{42}Ca 0.04 ±0.02%

^{40}Ca 2.71 ±0.02%

traces of other elements

A total of 326 runs were taken. This number includes 37 repeat runs. Repeat runs were usually separated from the original run by 10 hours, but a number of repeat runs were done with time gaps of 30 - 100 hours.

It is of interest that the presence of the oxygen on the ^{48}Ca target proved to be beneficial in that a great deal of accelerator time was saved since the ^{16}O angular distribution

and yield curve data were used by N. E. Davison in his study

of the ^{16}O + d reactions (Da 69).

(c) Polarized Deuteron Work

The polarized deuteron work was done in collaboration

with Dr. P. Quinn and Dr. W. Haeberli of the University of

Wisconsin, Madison, Wisconsin.

The experimental arrangement was very similar to the

one employed at the University of Alberta. Four moveable

detectors, 10° apart at a distance of 2.5" from the target

centre were used simultaneously. The detector collimators

were 0.7" high and 0.1" wide so that each detector subtended

a solid angle of about 1.1×10^{-2} steradians. The four

detectors were connected through a routing system to an ADC.

The output of the ADC was stored in the memory of the on-line

computer. Normalization factors for the various runs were

obtained through detection of the elastically scattered

deuterons in two detectors, placed at 13°. The monitor

detectors were set symmetrically above and below the scattering

plane. The sum of the counts of the monitors is insensitive

to small changes in the beam direction and is independent of

the vector analyzing power of the elastically scattered

deuterons (Yu 68). Pulses from the monitor counters were

fed into scalers. At the end of each run the four spectra

and the scaler numbers were written on magnetic tape. A

schematic drawing of the target chamber and associated

equipment is shown in Sc 68.

A self-supporting target of about 1.8 mg/cm^2

(obtained from Oak Ridge National Laboratory) was employed

for this part of the experiment. The target composition is

given below:

^{48}Ca	97.2	±0.05%
^{46}Ca	<0.02%	
^{44}Ca	0.10	±0.02%
^{42}Ca	0.04	±0.02%
^{40}Ca	2.71	±0.02%

traces of other elements

In order to reduce oxidation of this valuable target,

the sealed glass tube that contained the target was opened

inside an Argon-filled, transparent plastic bag that was

equipped with gloves. After the target had been mounted on

the target support, the bag was placed over the target support

hole in the top of the chamber (which had also been filled

with Argon) and the target support was lowered into the

chamber. The chamber was then quickly evacuated.

An angular distribution was taken at an incident

deuteron energy of 5.5 MeV to coincide with the 5.5 MeV

angular distribution taken at the University of Alberta. The

average beam current of the polarized deuteron beam at this

energy was about 0.4 nA. The dead time for any run was
less than 0.5%.

The polarized ion source has been described in Ha 67
and Cl 67. The source allows one t. use vector polarized
deuterons which have either spin up or spin down relative
to the scattering plane. One can therefore measure asymmetries
by taking two runs, one with spin up deuterons and one with
spin down deuterons, leaving the counters at the same angles.

3.3 Data Reduction

(a) Angular Distributions

The major target contaminants were ^{12}C and ^{16}O. In
addition to the Ca isotopes, very small quantities of ^{35}Cl,
^{88}Sr and ^{181}Ta, detected through their elastic scattering
peaks, were present on the target (see Fig. 3.2). The presence
of ^{88}Sr could be explained from the fact that Sr had been used
in a previous evaporation.

As an initial step in the data reduction, the monitor
sums of the ^{48}Ca elastic scattering peaks were taken for all
the runs. In order to achieve uniformity in the summing, the
following procedure was adopted. For a particular energy it
was ascertained that the peak was centred around the same
channel for all the runs. Constant sets of channels were
then used to take the peak sum and sample the background for

all the runs at that energy. The background was generally

of the order of 1 - 2% and the statistical error was usually

less than 1%. For each run the integrated charge was divided

by the peak sum. This ratio was constant within the statistical

errors and it was therefore decided that the integrated charge

could be used as a normalization factor for the angular

distributions. It is implicit in the above statement that no

normalization factor (different from 1) was needed between

the two target modes.

The reduction of the ground state data was a simple

procedure since no major contaminant peaks interfered with

this peak. The numerous ^{41}Ca peaks surrounding the ^{49}Ca

ground state peak were too small to be identified and formed

part of the rather smooth background. Sums were therefore

taken with a lightpen. The background was normally 1 - 2%

of the peak sum except at far forward angles where the background

was much larger. After background subtraction, the sums were

corrected for dead time and normalized for charge to give

relative cross sections. Statistical errors were typically

2 - 3% except at far forward angles where they were of the

order of 6%. Poorer statistics were taken at the far forward

angles to restrict the number of deuterons that entered the

counters.

Although the statistical errors are indicative of the

reliability of the data points, it was found from the repeat

runs that a more realistic experimental error of 5% should

be adopted instead of the 2 - 3% statistical error. This

increase in the error can be attributed to several error

sources: current integration, target non-uniformities,

uncertainty in the relative solid angles of the detectors

(about 1%) and the uncertainty in the detector angles (about

$0.2° - 0.3°$).

For the far forward angles a different procedure was

used to obtain sums and experimental errors. Where conditions

of high background and poor statistics prevail, it is normally

found that a number of equally acceptable ways of determining

background and sums will give quite different results. Several

sum and background determinations were therefore made with as

much objectivity as possible and the average of these sums

(after background subtraction) was used as the final sum. The

deviation from the average was then folded in with the statistical

error and the result rounded off to the nearest multiple of five

to give the experimental error.

Several contaminant peaks (^{14}N(0), ^{17}O(0) and ^{17}O(0.871))

interfered with the ^{49}Ca(2.028) peak at a number of angles.

Lightpen sums were taken at angles where the peak was free.

When a contaminant peak partially overlapped with the ^{49}Ca peak,

two analysis methods were used. The first one was to plot and

separate the two peaks by hand. The second one employed a

peak analysis program. It was found that if care was taken

the results from the two methods agreed very well. The background was nominally 4 - 6% of the peak sum; the statistical error was 2 - 3% and the experimental error was again set at 5%. At far forward angles the procedure outlined for the ground state was used. In this case, however, the situation was aggravated by the presence of the $^{17}O(0.871)$ peak on the high energy side so that experimental errors became quite large.

The elastic scattering peak of ^{48}Ca was free from contaminant peaks at back angles, except for a few far back angles at 5.5 MeV, where the $^{14}N(0)$ state interfered. Forward of 90° - 95° the ^{44}Ca elastic scattering peak merged with the ^{48}Ca elastic peak. The sum of the combined peaks was then taken and, with the assumption that the elastic scattering cross sections for ^{44}Ca and ^{48}Ca were the same, the contribution due to ^{48}Ca was extracted from the sum, according to the relative abundance figures given previously. In order to check the reliability of this procedure, the ^{44}Ca and ^{48}Ca peaks were summed as one peak at angles slightly back of 90° where the two peaks had not yet merged. The ^{48}Ca contribution was then found and this sum was compared to the sum of the ^{48}Ca peak alone. The two results always agreed to within 0.3%. Forward of 65° - 70° the ^{40}Ca peak merged with the ^{48}Ca peak as well. The same extraction procedure was used; the checks in this case showed agreement within 1.5%. In addition, it should be

mentioned that the elastic cross sections of ^{40}Ca (Le 68)
and ^{48}Ca are virtually identical at angles forward of 70°
at 5.0 MeV.

The above described extraction procedure relies on
the relative abundance figures supplied by Oak Ridge
National Laboratory as well as on the assumption that these
figures are unchanged after evaporation and deuteron bombard-
ment. From the work of T. A. Belote et al. (Be 68) and S. A.
Anderson et al. (An 68) it appears that the above assumption
is justified.

The background was nominally 1 - 2% of the elastic
peak sum; statistical errors were less than 1%. An experimental
error of 2.5% was assigned for angles greater than 65°. An
error of 5% was assigned for angles smaller than 65° for two
main reasons. First, because of the very rapid increase in
the elastic cross section at forward angles, the uncertainty in
the detector angles can give rise to errors estimated at 2 - 3%.
Secondly, it is felt that some additional error was introduced
with the extraction procedure when ^{40}Ca was present. The most
forward angle at which the ^{48}Ca sum could be taken was usually
determined by the merging of the ^{88}Sr peak with the Ca peak.

The 2.0 MeV proton elastic scattering was taken at four
angles between 70° and 90°. Each angle was repeated once.
The data was reduced in the same way as the deuteron elastic

scattering data. Background and statistical errors were less than 1% and an experimental error of 2.5% was assigned.

The conversion factor needed to convert the peak sums to absolute cross sections can now be determined as follows. Consider the equation

$$N_R = \frac{Q}{e} n \Omega \sigma_R \qquad 3.1$$

where N_R is the number of counts in the $^{48}Ca(p,p)^{48}Ca$ peak

Q is the total charge passing through the target

e is the charge of the proton

n is the number of ^{48}Ca nuclei per cm^2

Ω is the solid angle of the detector

σ_R is the ^{48}Ca Rutherford cross section for proton scattering

If Q, n and Ω are held constant, Eq. 3.1 can be written

$$N_R = \alpha \sigma_R \qquad 3.2$$

Since N_R is measured and σ_R is known, α can be determined. Eq. 3.2 can now be generalized to read

$$N = \alpha \sigma \qquad 3.3$$

Thus, since α is known, any peak sum can be converted to absolute cross sections. In this case, the average α, determined from the four angles, was used as the conversion factor.

It was assumed in this procedure that the proton scattering was purely Rutherford. Some credence is given to this assumption by a calculation of the elastic scattering with the proton parameters that were used in the DWBA calculations. These calculations show that the scattering is more than 99.2% Rutherford at 90°.

Listings of the angular distribution cross sections are presented in Appendix A. Graphs are shown in the next chapter.

(b) Yield Curves

The following table shows the approximate percentage background and statistical error for the peak sums:

Reaction	Background % of Peak Sum	Statistical Error (%)
$^{48}Ca(d,d)^{48}Ca$	~1	<1
$^{48}Ca(d,p)^{49}Ca(0)$	~1	2 – 3
$^{48}Ca(d,p)^{49}Ca(2.028)$	~3	2 – 3

A comparison of the repeat runs with the original runs showed that an experimental error of 2% should be assigned to the elastic scattering cross sections and an error of 4% to the (d,p) reaction cross sections. This comparison also showed that the average deviation was 0.3% and it was therefore concluded that the target had not deteriorated during the running period.

The conversion factor, needed to convert the peak sums to absolute cross sections, was obtained from the angular distributions. This conversion factor, an average over the seven angular distributions, had an r.m.s. error of 2.5%. The r.m.s. error is a strong indication of the relative error for the angular distribution cross sections over the 2.5 – 5.5 MeV energy range.

The ratio σ/σ_R was calculated for the elastic scattering yield curves. Since, at 65°, this ratio is 1.00 ± 0.03 below 3.2 MeV, the previous determination of the absolute cross sections is confirmed.

Because of the rather large number (~4400) of data points, no listing of the yield curve cross sections is given in this thesis. Graphs of the yield curves are shown in the next chapter. The elastic scattering is shown as the ratio σ/σ_R.

(c) Polarized Deuteron Work

The great care taken in transferring the target was repaid since contaminant peaks were negligible. Sums were taken with a lightpen and the following table gives the approximate percentage background and statistical error:

Reaction	Background % of Peak Sum	Statistical Error (%)
$^{48}Ca\ (d,d)^{48}Ca$	~2	<1
$^{48}Ca(d,p)^{49}Ca(0)$	~2	2 – 3
$^{48}Ca(d,p)^{49}Ca(2.028)$	~4 – 6	2 – 3

The analyzing power was calculated with the on-line computer from the formula

$$P_d^{(r)} = \frac{2}{3p}\ \frac{r-1}{r+1}\ [\ \frac{1}{1-\frac{\Delta p}{p}\ \frac{r-1}{r+1}}\ ] \qquad 3.4$$

where P_d refers to the analyzing power of the elastic scattering and P_d^r refers to the analyzing power of the (d,p) reactions. This formula may be simply derived from the basic formula (Yu 68)

$$\sigma_{\uparrow,\downarrow}(\theta) = \sigma_{unp}(\theta)\ [1 \pm \frac{3}{2}P_{\uparrow,\downarrow}P_d^{(r)}(\theta)] \qquad 3.5$$

(the arrows ↑ and ↓ indicate deuterons with spin up and spin down respectively) with the substitutions

$$r = \frac{S\uparrow}{S\downarrow} \qquad \text{S is the peak sum normalized for charge}$$

$$P_\uparrow + P_\downarrow = 2p \qquad \text{p is the average beam polarization}$$

$$P_\uparrow - P_\downarrow = 2\Delta p \qquad \text{2Δp is the difference between the spin up and spin down polarization}$$

The formula from which relative cross sections can be calculated may also be derived from Eq. 3.5 and is given by

$$\sigma = \frac{1}{2} [S_\uparrow + S_\downarrow] [1 - \frac{\Delta p}{p} \frac{r-1}{r+1}] \qquad 3.6$$

It should be noted that it has been assumed in Eq. 3.5 that no tensor polarization is present in the beam.

Because of the finite height of the detectors, two corrections must be considered. First, the average detector angle $\bar{\theta}$ must be determined. From Fig. 3.3 (top) it is seen that

$$d_o \cos\theta_o = \sqrt{d_o^2 + y^2} \cos\theta_y$$

$$\therefore \quad \cos\theta_y = \frac{d_o}{\sqrt{d_o^2 + y^2}} \cos\theta_o$$

Thus θ_y may be determined for any y. If the detector height is divided into n strips of equal height, $\bar{\theta}$ is given by

$$\bar{\theta} = [\theta_o + \sum_1^n \theta_y]/n + 1$$

In this case n = 18 was used.

Secondly, a correction must be applied to the analyzing power since the beam polarization is given by p cosϕ, where the angle ϕ is shown in Fig. 3.3 (bottom). It is therefore necessary to average the beam polarization over cosϕ when finite height detectors are used, i.e., the average beam polarization p' = p $\overline{\cos\phi}$. Thus the average $P_d' = P_d/\overline{\cos\phi}$ (See Eq. 3.4). The angle ϕ and thus $\overline{\cos\phi}$ may be easily determined from Fig. 3.3 since $\ell = d_o \sin\theta$

$$\therefore \quad \phi = \tan^{-1} \frac{h}{2d_o \sin\theta}$$

Figure 3.3   Explanatory drawing for the determination

of the average scattering angle $\bar{\theta}$ (top)

and the correction factor $\overline{\cos\phi}$ (bottom)
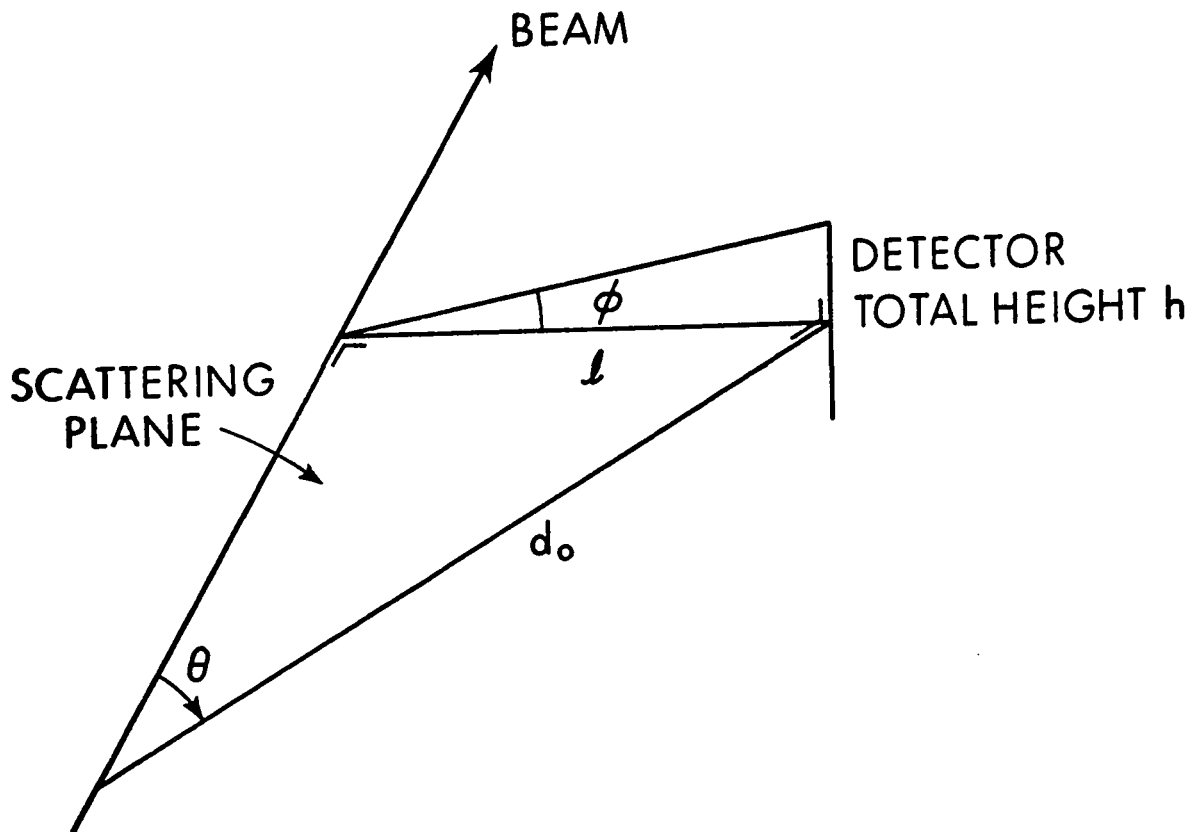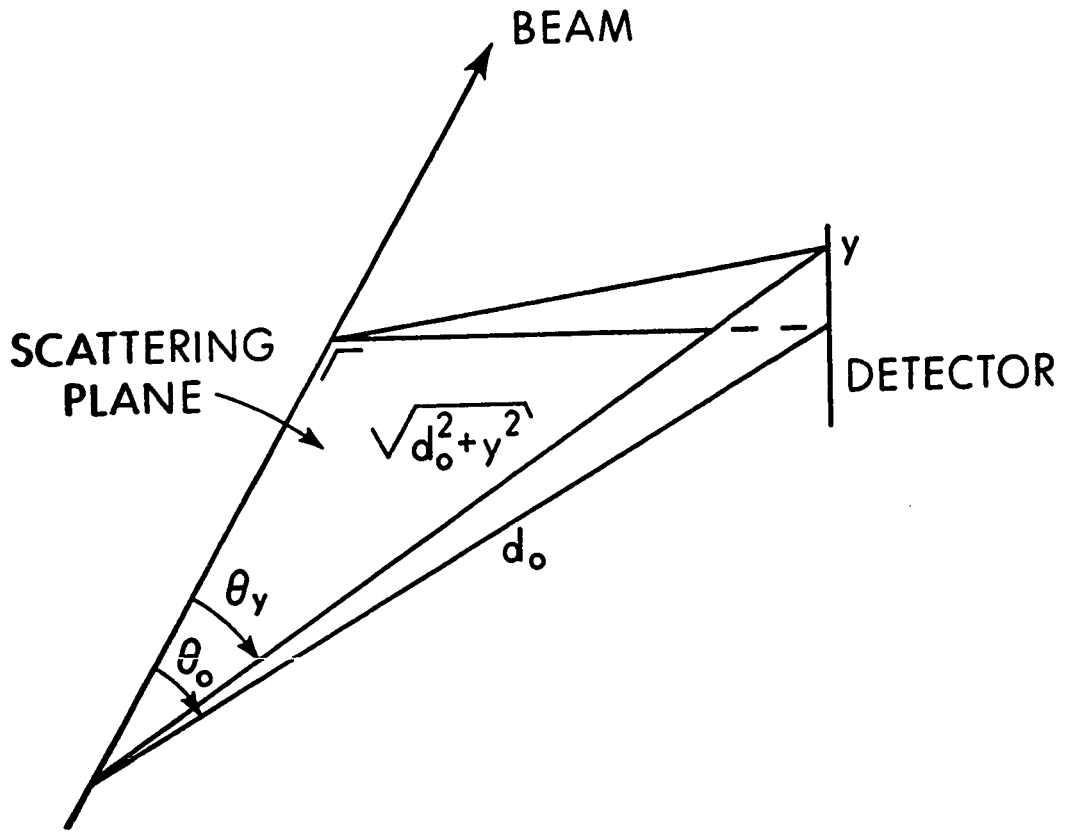
CHAPTER 4

ANALYSIS

4.1 Compound nucleus calculations

A short account of the compound nucleus calculations
will be given here. The calculations were performed with
the program HAUSER (Sm 65) modified by N. E. Davison (Da 69a).

The statistical model requires that all energetically
allowed decay channels of the ^{48}Ca + d compound nucleus be
known. Unfortunately, only the low lying states in the
residual nuclei are known so that a statistical level density
distribution had to be assumed for the higher lying levels.
The level density formula used in the program is of the
form $\log N(E_x) = a + b \sqrt{E_x}$ where $N(E_x)$ is the total number
of levels up to E_x and E_x is the excitation energy.

It was found that the major uncertainty in the results
was introduced by the level densities. Two sets of calculations
were therefore done, one with level densities that were slightly
high and one with level densities that were slightly low. The
results of these calculations fell approximately 40% on either
side of the original results, thus providing some estimate of
the relative uncertainty.

The calculations showed that the compound nucleus cross
sections for the elastic scattering were negligible compared
to the experimental cross sections. In the case of the ground

state the compound nucleus cross sections were less than

10% of the smallest measured cross sections at deuteron

bombarding energies between 4.0 MeV and 5.5 MeV and less

than 5% at the lower energies. For the first excited state

the compound nucleus cross sections were less than 2% of

the smallest measured cross sections over the entire energy

range.

4.2 Optical Model Analysis

Two computer codes were used in parallel for the

optical model analysis. The first code, PEREY, written by

Perey (Pe 63, Ob 66) did not allow the use of a spin-orbit

potential for spin 1 particles; the second code, SNOOPY[*], did

allow the use of a spin-orbit potential but did not contain

the non-locality correction. The specific results quoted

in this chapter were obtained with the code SNOOPY. The

findings from the two codes were very similar (except, of

course, findings relating to the spin-orbit potential) so that

statements made in this section apply to both codes.

It was felt that it was in the nature of the optical

model that a broad and continuous range of parameter sets

---

[*]Obtained from W. Haeberli, University of Wisconsin, Madison, Wisconsin.

should exist which would fit the data about equally well,
i.e., χ^2, the goodness-of-fit parameter would vary slowly
and continuously (see Fig. 4.1). An initial series of
calculations was therefore performed in which only the
central potentials were used to reduce the complexity of
the situation. In these calculations the real potential
well depth V was gridded from 90 to 130 MeV in steps of
5 MeV, each step followed by a search over other parameters
(this type of calculation will be referred to as a grid-
search). Several 2, 3, 4 and 5 parameter combinations
were used for the searched parameters. From these calculations
it was found that a search over any 2 or 3 parameter combination
was insufficient and that a five parameter search was erratic
in the sense that the program tended to get "lost" in
parameter space, and would find its way into unphysical
regions. A four parameter search, however, proved to be
both necessary and sufficient to produce the anticipated
continuous behaviour. It was also found that three parameters
belonging to the same potential should not be searched simul-
taneously in order to avoid erratic results.

A total of six parameters must be determined for the
two central potentials. Since V is to be gridded, it follows
from the above findings that one parameter belonging to the
imaginary potential cannot be searched but must be fixed or

gridded. The choice of the imaginary diffuseness a_i as

the "fixed" parameter was governed by the following

considerations: that the imaginary radius r_i had been

found to be a necessary search parameter and that the

imaginary well depth W was expected, from the results of

Schwandt and Haeberli (Sc 69), to vary with incident

deuteron energy, so that a search over W would be preferable.

The central parameters to be searched simultaneously

are therefore:

the real radius r_o

the real diffuseness a_o

the imaginary well depth W

the imaginary radius r_i

The starting point for the optical model analysis

was the 5.5 MeV data since it included the deuteron polari-

zation which is needed to determine the spin-orbit potential.

The inclusion of the spin-orbit potential means that now a

total of nine parameters must be determined. A preliminary

set of searches over the combined cross section and polari-

zation data established the following three points:

1) The fit to the polarization data was very poor

(see Fig. 4.3). The χ^2 belonging to the

polarization data is therefore very high and

cannot be used as a convergence criterion for

optimum fit.

2) The spin-orbit parameters affect the cross section χ^2 very little (see Table 4.2) and have their major effect on the polarization fit in the sense that they are needed to generate the polarization. Points 1) and 2) therefore show that the objective approach of searching over the spin-orbit parameters to establish a best fit is meaningless and that a subjective, i.e., visual, approach must be used to fit the polarization data. It should be pointed out, however, that because of this approach, the polarization fit is rather insensitive to small changes in the spin-orbit parameters.

3) A search over the four previously mentioned central potential parameters (spin-orbit parameters fixed) produces a basically correct shape for the polarization. In other words, the central potential parameters affect the fit to the polarization data greatly and these parameters, properly optimized, can predict the basic shape of the polarization.

Similar findings have been reported by Schwandt and Haeberli (Sc 69).

In view of the above findings, the 5.5 MeV data was analyzed with a grid-search in which V, a_i, V_{SO}, r_{SO}, and a_{SO} were gridded and r_o, a_o, W and r_i were searched. The spin-orbit parameters were then selected on the basis of best subjective fit to the polarization data. The central potential parameters were of course determined by the minimum χ^2 for the cross section. The results for the central potential parameters are shown in Fig. 4.1, where the parameters r_o, a_o, W, r_i and a_i are plotted versus V. It should be noted that identical results for the searched parameters were obtained from three different sets of starting values. These results are therefore independent of a possible bias in the starting values.

The spin-orbit parameters were found to be constant with V within the subjective approach that was used. The values for these parameters are

$$V_{SO} = 10.0 \text{ Mev}$$
$$r_{SO} = 0.91 \text{ fm}$$
$$a_{SO} = 0.60 \text{ fm}$$

The six energies between 2.5 and 5.0 MeV were analyzed with a grid-search in which V and a_i were gridded and r_o, a_o, W and r_i were searched. The spin-orbit parameters were held constant at the above stated values, since no polarization data, necessary to determine these parameters, was available at these energies. The behaviour of the central

Figure 4.1   The central potential parameters r_o, a_o, W, r_i, a_i and the goodness-of-fit parameter χ^2 as a function of the real well depth V for the deuteron energy $E_d = 5.5$ MeV.
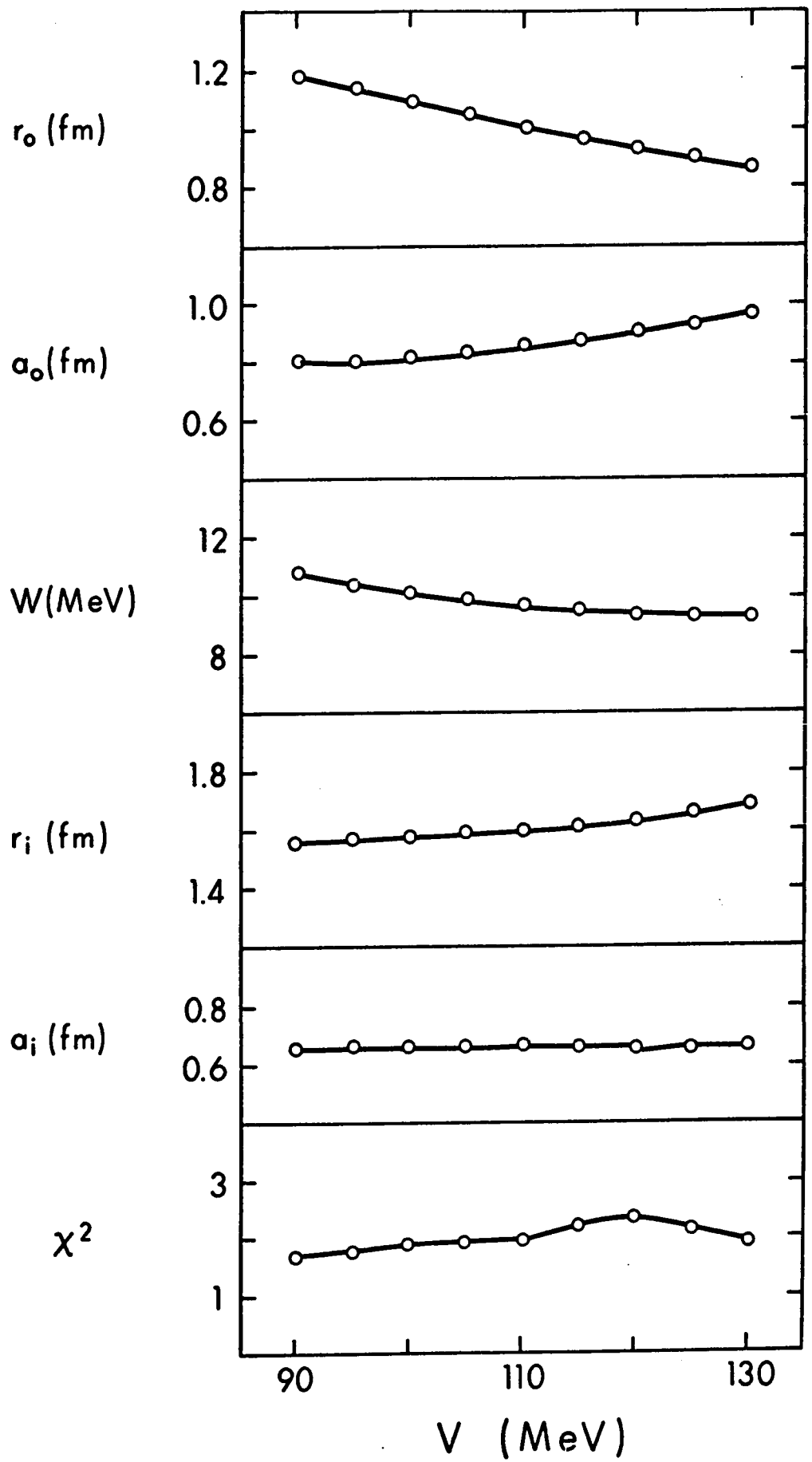
potential parameters was similar to the behaviour at 5.5 MeV as shown in Fig. 4.1 Fits to the cross section and polarization data are shown in Fig. 4.2 and Fig. 4.3 as solid lines.

It is seen from Fig. 4.1 that there is really no preferred set of optical model parameters on the basis of χ^2. A number of DWBA calculations were therefore performed in which several deuteron real well depths with their associated parameter sets were used. These calculations showed that the first stripping peak of the ground state was best reproduced for a real deuteron well depth of 90 to 100 MeV. A well depth of 95 MeV was therefore adopted. The parameters belonging to a real well depth of 95 MeV at the various energies are listed in Table 4.1. These parameters will be referred to as the proper parameters.

The ambiguities mentioned in Chapter 2 are clearly seen in Fig. 4.1; r_o decreases and a_o increases with increasing V etc. It is difficult to determine what parameter combination constitutes an ambiguity or what correlations exist between the six central parameters. It would be of interest, however, to determine such correlations in order to derive general rules for the behaviour of the central parameters.

Figure 4.2   Plots of the ratio σ/σ_R versus the centre-
of-mass angle for the reaction $^{48}Ca(d,d)^{48}Ca$.
The solid and dashed lines are the Optical
Model fits to the data calculated with the
proper and average deuteron parameters
respectively.
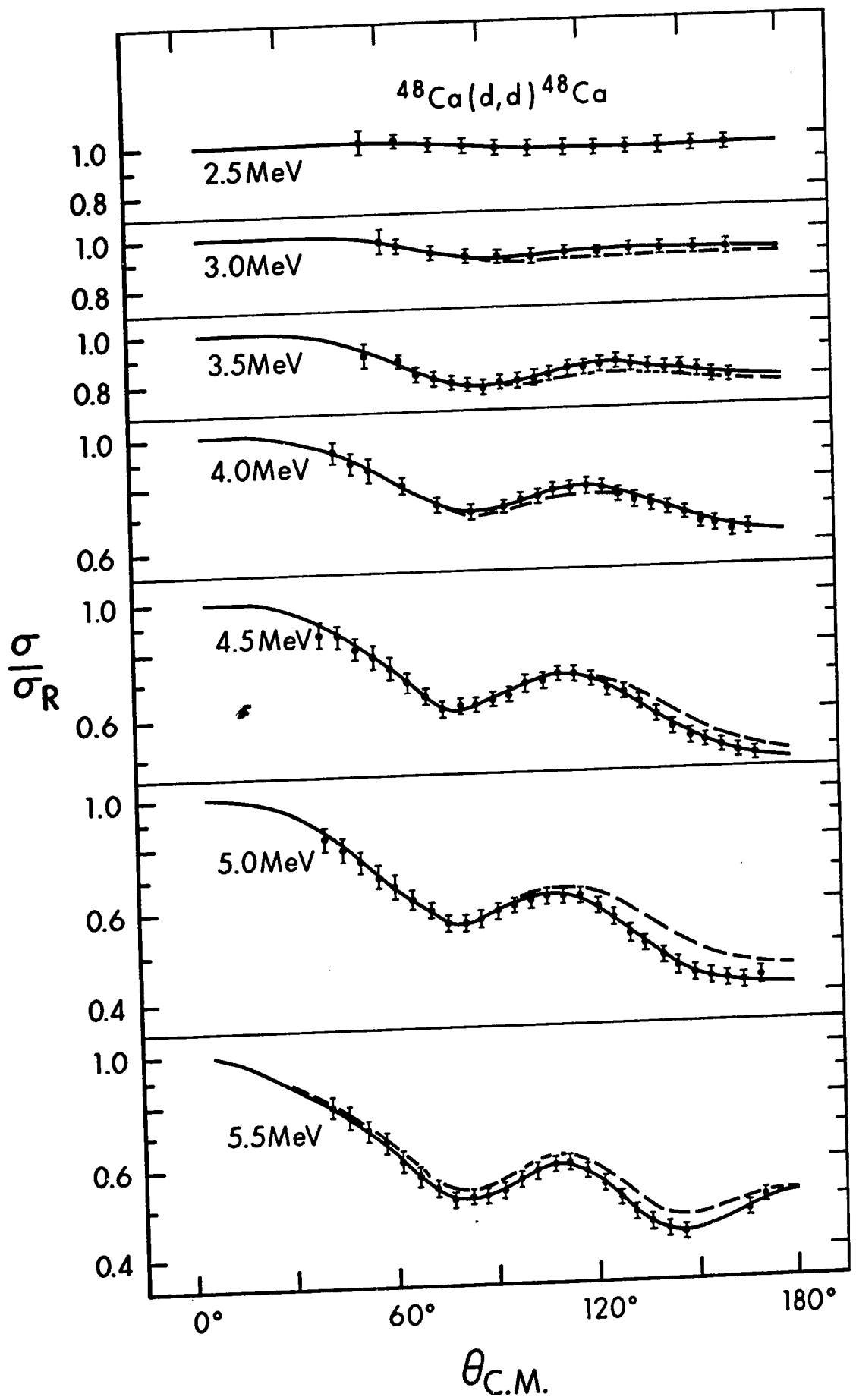
$^{48}Ca(d,d)^{48}Ca$

Figure 4.3   Angular distribution of the polarization (analyzing power) of the ^{48}Ca(d,d)^{48}Ca reaction. E_d = 5.5 MeV. The solid line is the Optical Model fit to the data.

$^{48}Ca(d,d)^{48}Ca$

$E_d = 5.5\ MeV$
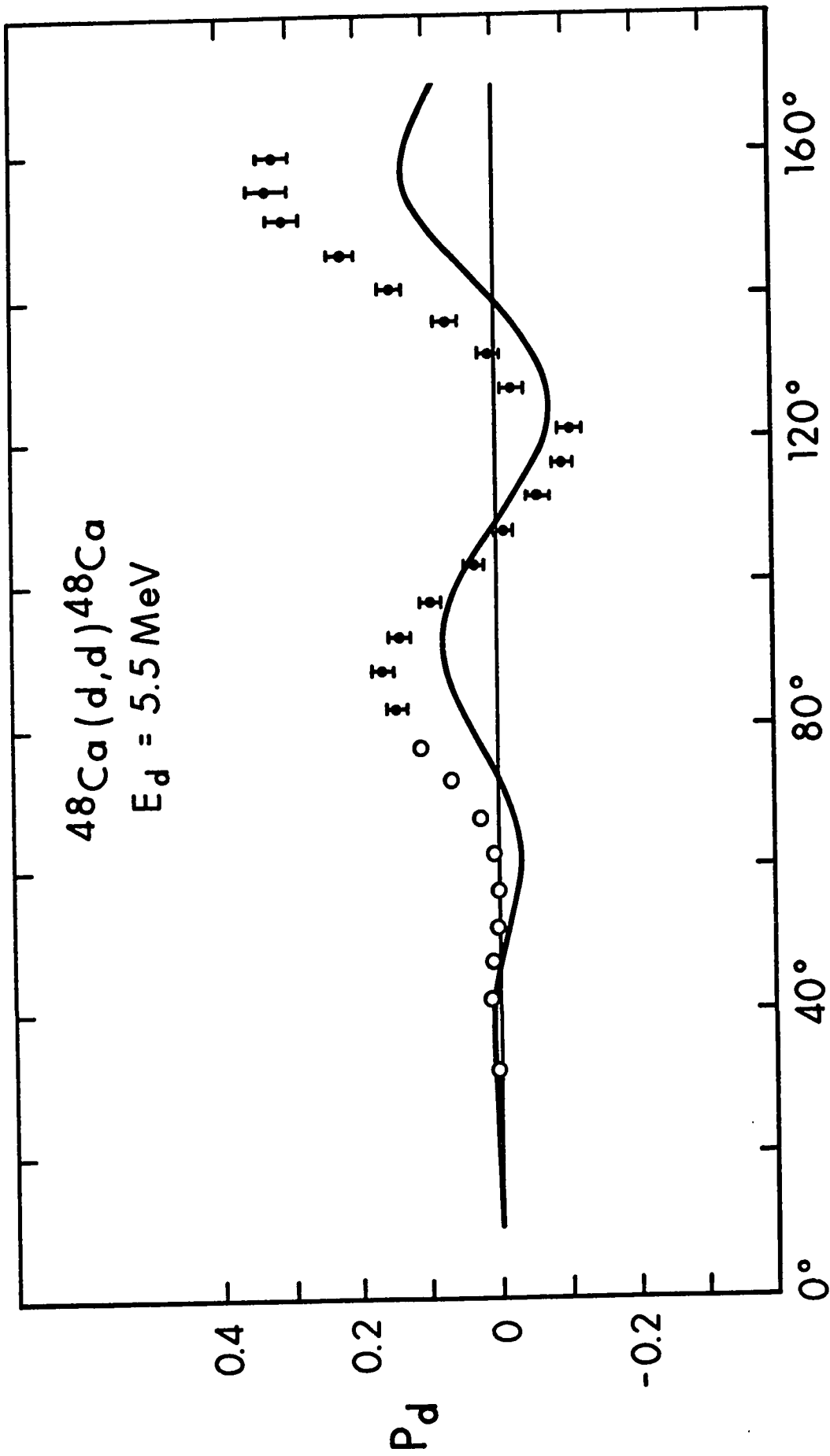
TABLE 4.1

PROPER OPTICAL MODEL PARAMETERS

E_d (MeV)	r_o (fm)	a_o (fm)	W (MeV)	r_i (fm)	a_i (fm)
2.5	1.11	0.74	6.47	1.54	0.66
3.0	1.18	0.66	7.21	1.60	0.66
3.5	1.16	0.71	6.05	1.68	0.67
4.0	1.19	0.67	8.37	1.46	0.66
4.5	1.18	0.71	9.18	1.48	0.66
5.0	1.22	0.64	13.8	1.26	0.65
5.5	1.14	0.81	10.4	1.57	0.66

At all deuteron energies:
$$V = 95.0 \text{ MeV}$$
$$V_{SO} = 10.0 \text{ MeV}$$
$$r_{SO} = 0.91 \text{ fm}$$
$$a_{SO} = 0.60 \text{ fm}$$

A set of calculations was performed in which each parameter was changed in turn by 1% from its proper value and the percentage change in χ^2 was calculated. The results for deuteron energies of 2.5, 4.0 and 5.5 MeV are shown in Table 4.2. A change of less than 1% in χ^2 was used as a search cut-off and it appears therefore from the first column in Table 4.2 that even at 2.5 MeV all searched parameters were determined to 1% or better, i.e., a change of 1% in any one parameter could not effect an improvement of 1% in χ^2. It is clear, however, that the parameters are less critically determined as the energy decreases, or, in other words, that the minimum in χ^2 space becomes less pronounced.

The last column in Table 4.2 shows the percentage change in χ^2 averaged over 4.0 and 5.5 MeV. This figure can be seen as a figure of merit for that parameter in the sense that the higher this figure, the more effective this parameter is in the fitting procedure. These figures substantiate the choice of the four central parameters that were searched. It should be noted that the change in χ^2 was always an increase. It was therefore also verified that indeed a minimum χ^2 had been obtained with the proper parameters.

The proper central parameters are plotted versus the incident deuteron energy in Fig. 4.4. It is seen that in order to obtain the average parameters, simple averages can be taken for r_o, a_o and a_i. In the case of r_i the scatter

TABLE 4.2

INCREASE IN χ^2 FOR 1% CHANGE IN PARAMETER

Parameter Changed by 1%	E_d = 2.5 MeV Increase in χ^2 (%)	E_d = 4.0 MeV Increase in χ^2 (%)	E_d = 5.5 MeV Increase in χ^2 (%)	Average Increase in χ^2 (%)
V	6	345	506	425
r_o	9	1233	1634	1433
a_o	13	291	676	483
W	1	14	27	21
r_i	5	198	1167	683
a_i	2	15	27	21
V_{SO}	0	1	1	1
r_{SO}	0	1	1	1
a_{SO}	0	0	0	0

Figure 4.4   The proper central potential parameters r_o, a_o, W, r_i and a_i as a function of the incident deuteron energy. The real well depth $V = 95$ MeV. The solid lines show the average parameters.
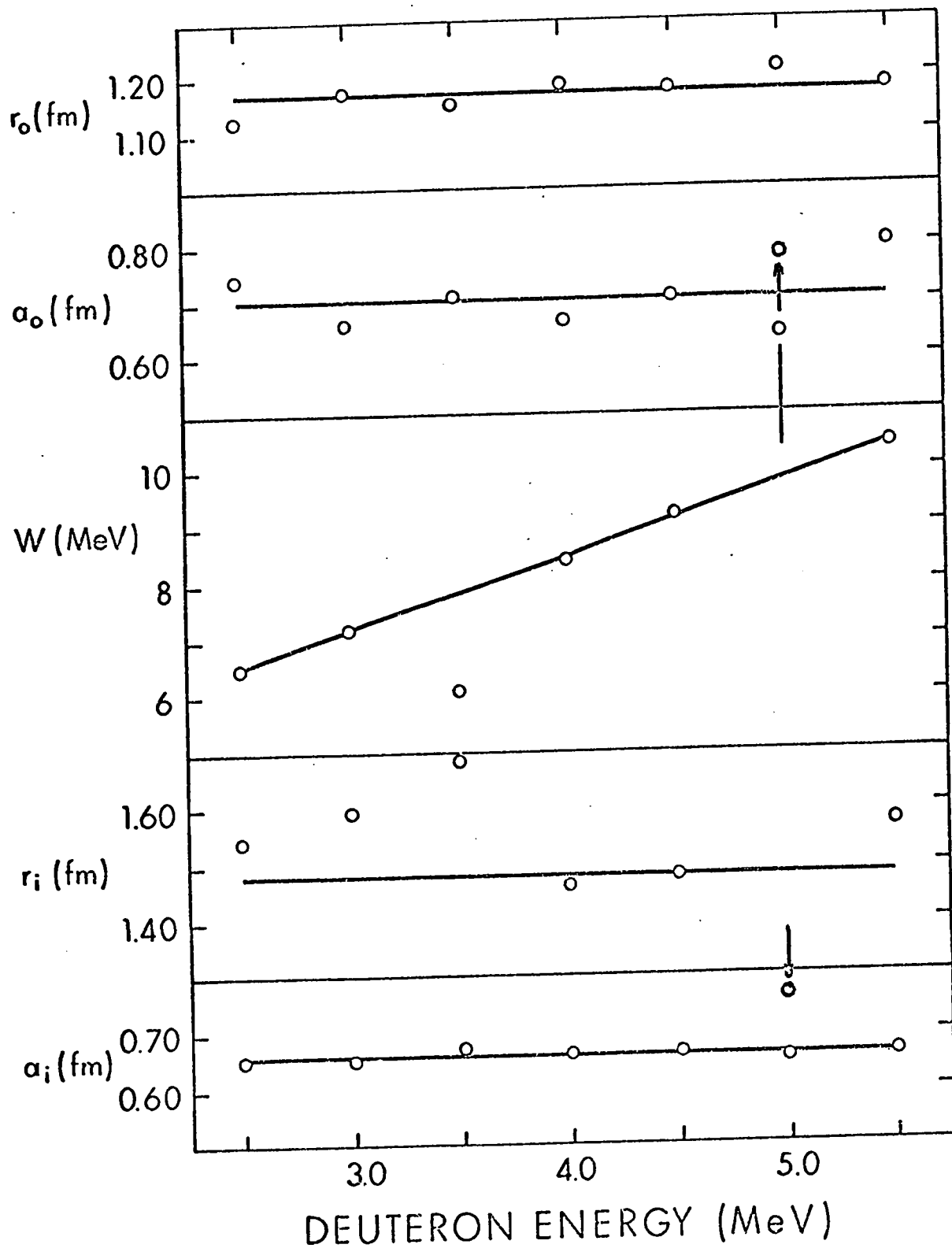
in the points is quite large without a real trend. The value of r_i at 4.5 MeV was adopted as the "average" value since at this energy the other proper parameters are virtually identical with the average parameters. The behaviour of the imaginary well depth can be given by the straight line equation $W = (1.3\ E(MeV) + 3.3)$ MeV. The averages are shown as solid lines in Fig. 4.4. The quite smooth behaviour of the proper central parameters over the energy range is expected on the basis of the smooth behaviour of the elastic scattering yield curve, which is shown in Fig. 4.5.

The average deuteron optical model parameters for the energy range 2.5 – 5.5 MeV are thus

$V = 95.0$ MeV $W = (1.3\ E(MeV) + 3.3)$ MeV $V_{SO} = 10.0$ MeV

$r_o = 1.17$ fm $r_i = 1.48$ fm $r_{SO} = 0.91$ fm

$a_o = 0.71$ fm $a_i = 0.66$ fm $a_{SO} = 0.60$ fm

The elastic scattering angular distributions calculated from the average parameters are shown as dashed lines in Fig. 4.2.

In order to determine the possible energy dependence of the real well depth, a search was made over V at the various energies with all other parameters fixed at their average values. The values of V so determined were all in the range 95 ± 1 MeV with no apparent trend and it was concluded that no energy dependence of V could be established from the present data.

Several comments regarding the Optical Model analysis must be made. From Fig. 4.2 it is clear that the average

Figure 4.5   Plots of the ratio σ/σ_R versus the incident deuteron energy for the reaction $^{48}Ca(d,d)^{48}Ca$.

^{48}Ca(d,d)^{48}Ca

65°

90°

115°

145°

165°

$\frac{\sigma}{\sigma_R}$

1.00 0.75 0.50

DEUTERON ENERGY (MeV)

3.0   4.0   5.0   6.0
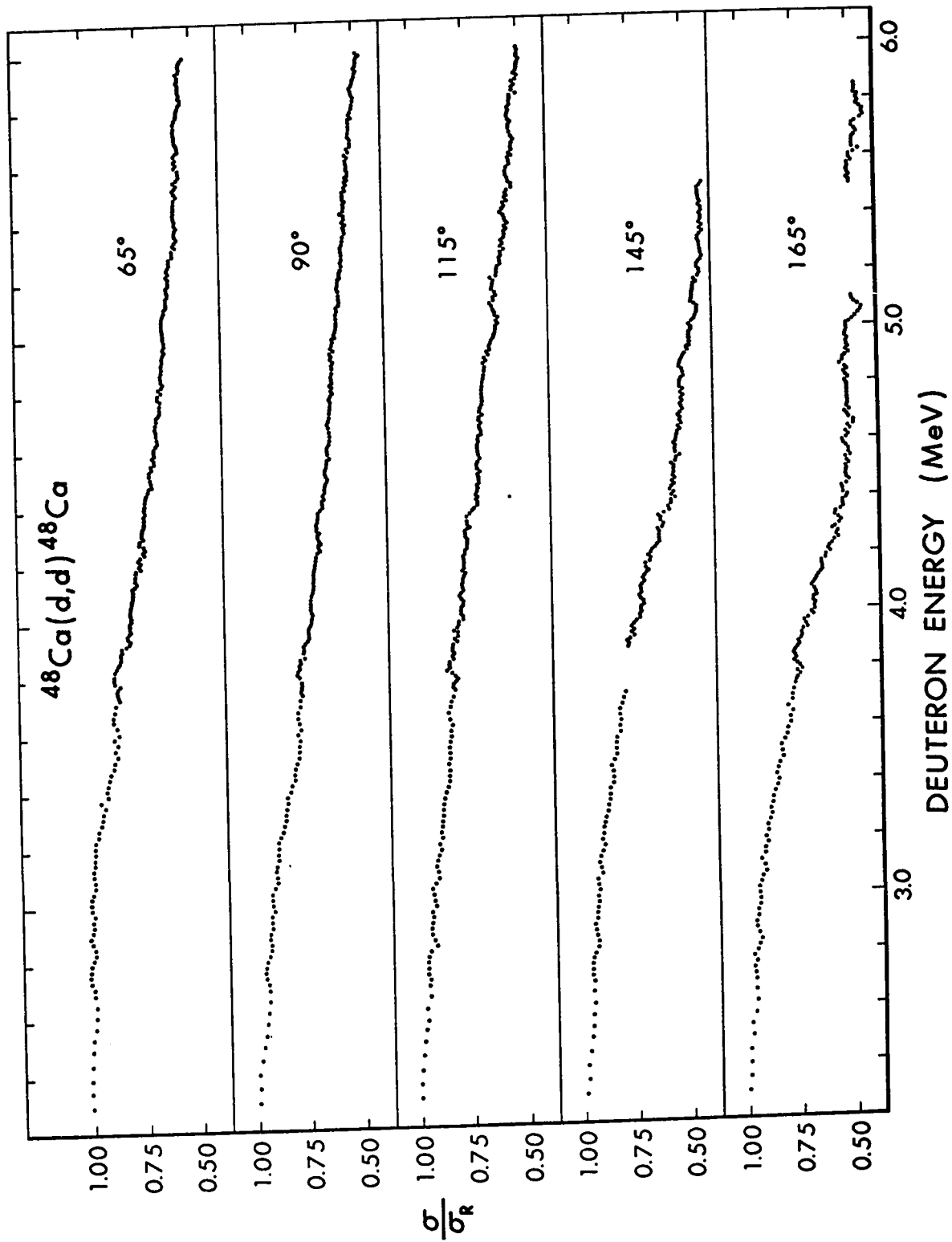
deuteron parameters do not fit the data as well as the proper parameters. It should be noted, however, that only the magnitude is affected, whereas the proper phase is preserved. As a matter of interest, the average deuteron parameters for ^{40}Ca of Schwandt and Haeberli (Sc 69) were used to generate the ^{48}Ca elastic scattering at 5.5 MeV. It was found that the angular distribution so calculated was greatly different in phase. It appears therefore that deuteron parameters appropriate to one nucleus can not be used with another nucleus. It is hoped, however, that an extensive study of deuteron elastic scattering may provide a set of generally applicable deuteron parameters.

From their study of ^{40}Ca deuteron elastic scattering, which included deuteron polarization, Schwandt and Haeberli found that the energy dependence of the real well depth V is weak at low energies, whereas the imaginary well depth W has a strong energy dependence at low energies. The findings of this study agree with these results. They also found that even with the inclusion of a tensor force, the deuteron polarization was poorly fitted, particularly at low energies. A similarly poor fit to the polarization is obtained in this work and it must be concluded that there are still basic deficiencies in the Optical Model.

Two comments should be made regarding the inclusion of the spin-orbit potential in the analysis. First, the inclusion of the spin-orbit potential decreases χ^2 by about a factor of two, so that indeed a better fit to the data is obtained. Secondly, in Fig. 4.1, which shows the central parameters as a function of the real well depth V, only the range V = 90 - 130 MeV is shown. It should be mentioned, however, that the range of V that was investigated stretched from 40 MeV to 150 MeV. If no spin-orbit potential was included, acceptable smooth sets of parameters, similar to the ones shown in Fig. 4.1, could be generated between 40 MeV and 90 MeV as well as between 130 MeV and 150 MeV. With the inclusion of the spin-orbit potential, however, the χ^2 in these regions increased sharply and no smooth trend could be detected in the parameters. In addition, the predicted polarization in these regions is exactly out of phase with the data. It was therefore concluded that on the basis of the elastic scattering data (including polarization) the deuteron real well depth should be of the order of 100 MeV, in accordance with the idea that the deuteron well depth be approximately the sum of the well depths for the proton and the neutron.

4.3 DWBA Analysis

The DWBA calculations were carried out with the computer

program DWUCK[*]. This program calculates the wavefunctions

of the three particles participating in the reaction: the

incident deuteron, the outgoing proton and the absorbed

neutron. A total of 21 potential parameters are needed as

input for such a calculation, nine each for the deuteron and

the proton and three for the neutron. As explained before,

the deuteron and proton parameters are obtained from an

analysis of their respective elastic scattering data and are

as such determined. There is uncertainty, however, about

the neutron parameters.

The neutron wavefunction is that of a particle moving

in a real central potential of Woods-Saxon form and a spin-orbit

potential of the Thomas form. The depth of the central well

is adjusted by the program so that the binding energy of the

neutron in the well is equal to the experimental separation

energy; the spin-orbit radius and diffuseness are the same

as for the central well. Thus there are three undetermined

parameters: the radius r, the diffuseness a and the depth V_{so}

of the spin-orbit potential. From a series of calculations

the following observations were made:

1) changes in the three parameters did not affect the
   shape of the predicted angular distributions but did
   affect the magnitude of the cross section;

---

[*]Obtained from P. D. Kunz, University of Colorado.

2) an increase of 1% in the radius r caused an increase

of about 3% in the cross section; an increase of 1%

in the diffuseness a caused an increase of about 1%

in the cross section. Thus r is three times more

effective than a in this respect and there exists an

ambiguity $ra^n = C$ where C is a constant and $n \approx 0.3$.

Removal of the spin-orbit potential caused a decrease

in the cross section of about 3%;

3) the real well depth as adjusted by the program was

mostly affected by the radius r. In addition, the

well depths for the ground and first excited states

were different for the initial set of parameters,

but each well depth changed by a different amount

for a change in the radius r.

It was then argued that since both the ground state and

the first excited state are $\ell = 1$ states, the real well depth

should be the same for both states and that the difference in

the binding energy (in the Shell Model this is referred to as

the splitting of the $j = 3/2$ and $j = 1/2$ states) should be

accounted for by the spin-orbit potential.

Since the radius r is the most effective of the parameters

and because of the previously mentioned ra^n ambiguity, the spin-

orbit strength and the diffuseness were fixed at 8 MeV and 0.65

fm respectively and r was adjusted until the real well depth

was the same for both states. Identical depths of 54.4 MeV
were obtained for a radius r = 1.15 fm. Thus the neutron
parameters used in all final calculations are:

$$r = 1.15 \text{ fm}$$

$$a = 0.65 \text{ fm}$$

$$V_{SO} = 8 \text{ MeV}$$

Since ^{49}Ca is unstable, the proton parameters belonging
to ^{48}Ca were used. These parameters have been determined by
Marinov, Lee and Schiffer (Ma 66) from their proton elastic
scattering data. The proton parameters are listed below:

$V = 51.4$ MeV	$W = 8.6$ MeV	$V_{SO} = 7.5$ MeV
$r_o = 1.24$ fm	$r_i = 1.19$ fm	$r_{SO} = 1.24$ fm
$a_o = 0.63$ fm	$a_i = 0.64$ fm	$a_{SO} = 0.63$ fm

DWBA calculations were performed at each of the seven
deuteron energies with both the proper and the average
deuteron parameters; finite range and non-locality corrections
were included in all calculations. The experimental and
calculated angular distributions of the ground state are
shown in Figs. 4.6 and 4.7, where the solid and dashed lines
refer to the proper and average deuteron parameters respectively.
The calculated angular distributions were normalized to fit
at the largest experimental cross sections. In order to extend
the range of this study, the ground state angular distribution
at $E_d = 7.0$ MeV, taken from the work of Belote et al. (Be 68),
has been included. It is shown in Fig. 4.7 where the predicted

Figure 4.6   Angular distributions of the ^{48}Ca(d,p)^{49}Ca(0)

reaction.

Figure 4.7   Angular distributions of the ^{48}Ca(d,p)^{49}Ca(0)

reaction.

In both figures the lines are the DWBA

predictions. The solid and dashed lines

refer to the proper and average deuteron

parameters respectively.

$^{48}Ca(d,p)^{49}Ca(0)$

$^{48}Ca(d,p)^{49}Ca(0)$
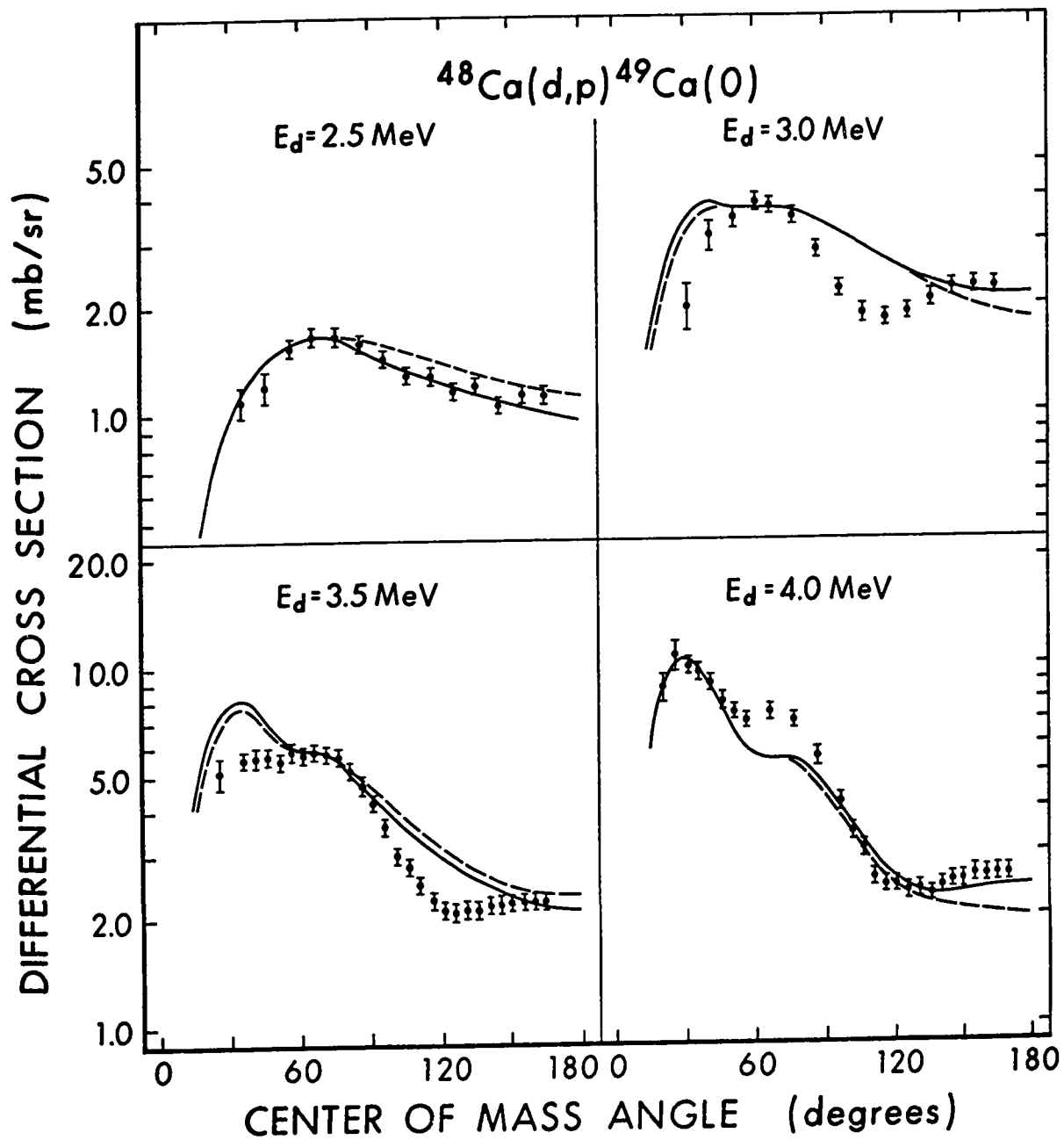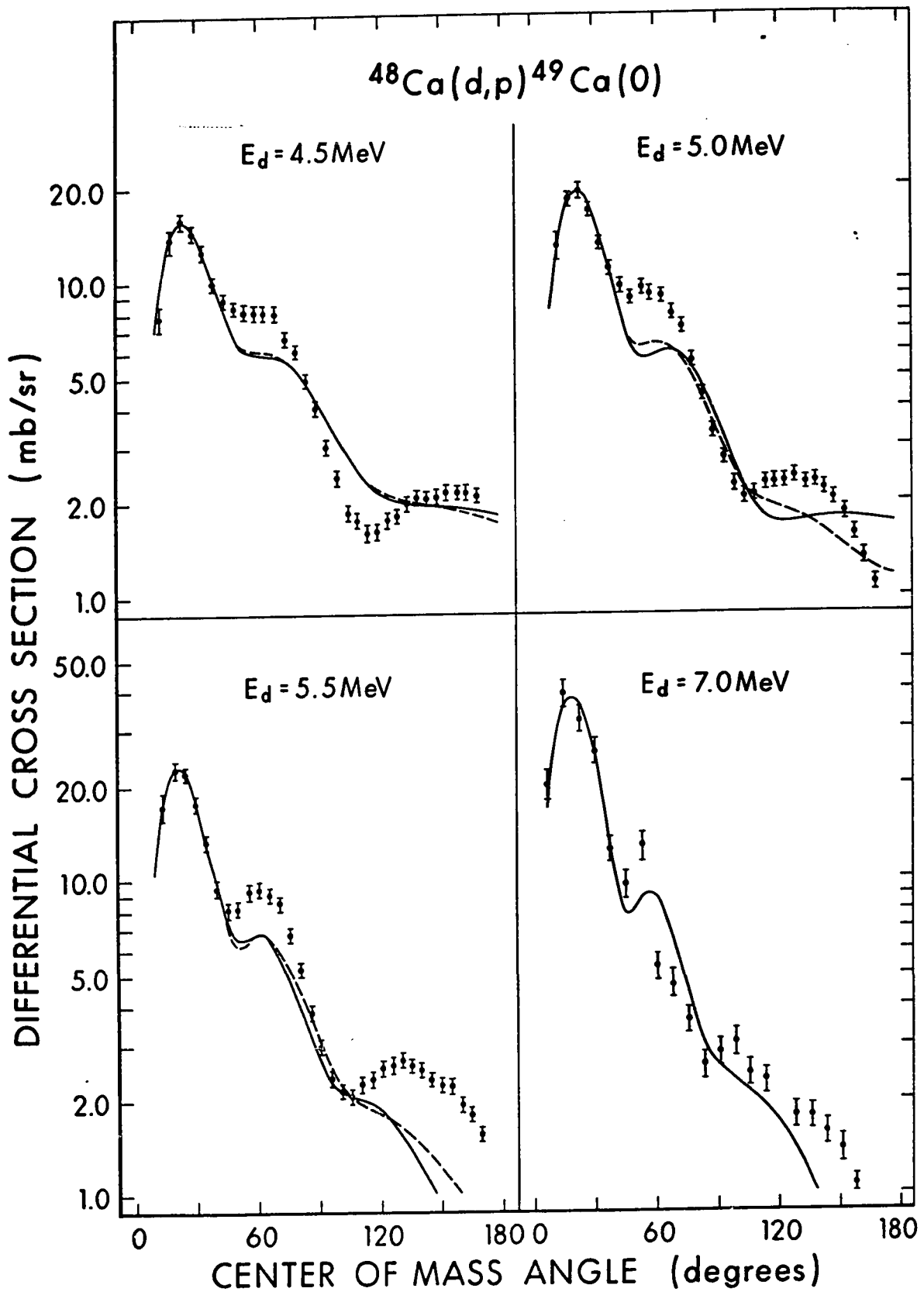
angular distribution has been calculated with the average deuteron parameters.

It is seen from Figs. 4.6 and 4.7 that the shapes for the two sets of parameters are almost identical, except at back angles and that no preference can be given to either set on the basis of shape.

The DWBA calculations reproduce the ground state angular distributions well at forward angles, except at E_d = 3.0 and E_d = 3.5 MeV. At these energies DWBA still predicts a slight forward stripping peak, whereas this peak has disappeared below E_d = 4.0 MeV in the data. At the back angles the fit to the ground state is poor but this is to be expected since the yield curves (Fig. 4.8) show large fluctuations at angles greater than 90°. It should be noted, however, that DWBA calculations with the average deuteron parameters do predict the overall shape of the yield curve at the back angles (see Fig. 4.8). The major failure of DWBA is the inability to reproduce the second stripping peak at about 65°. This peak is indicated by the calculations but the predicted cross sections are always too small (Figs. 4.6, 4.7 and 4.8). Several attempts to improve this situation through small changes in one or two parameters met with no success and it must therefore be concluded that DWBA theory fails in this respect.

Figure 4.8   Yield curves of the ^{48}Ca(d,p)^{49}Ca(0)

reaction. The solid lines are the

DWBA predictions calculated from the

average deuteron parameters.

$^{48}Ca(d,p)^{49}Ca(0)$

DEUTERON ENERGY (MeV)

DIFFERENTIAL CROSS SECTION (mb/sr)
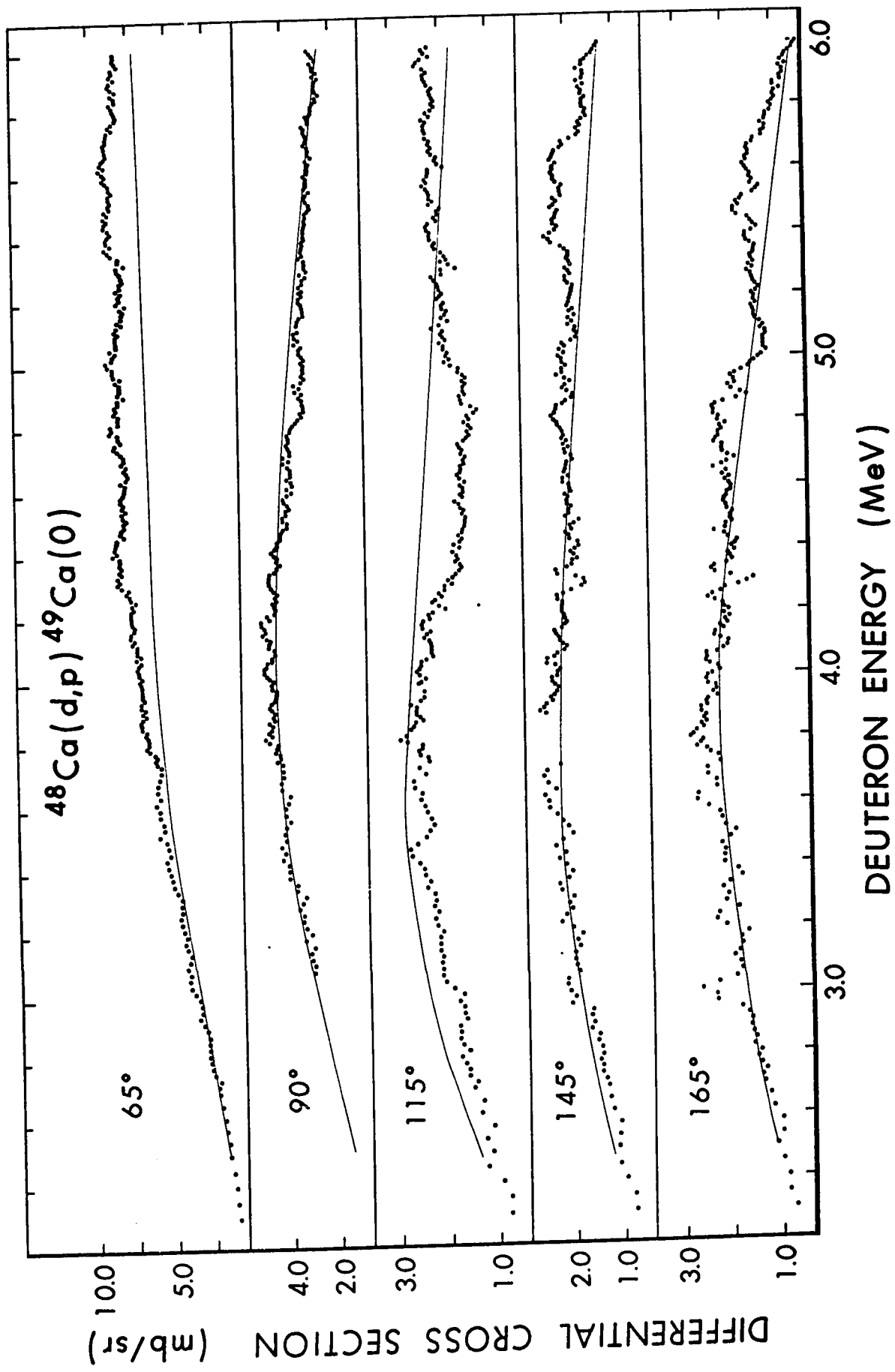
The angular distributions for the first excited state are shown in Figs. 4.9 and 4.10. It is seen that the DWBA calculations reproduce the data extremely well except around 65° (the second stripping peak) where the predicted cross sections are slightly too small. Although again the differences in shape between the two sets of deuteron parameters are small, it appears in this case that the average deuteron parameters provide a slightly better fit to the data, particularly at E_d = 5.5 MeV. The fluctuations in the yield curve of the first excited state (Fig. 4.11) are smaller than those in the ground state yield curve and the DWBA predictions for the yield curves are remarkably good at all angles.

Fig. 4.10 includes the predicted angular distribution for the first excited state at E_d = 7.0 MeV. A comparison of the predictions for the ground state and first excited state at E_d = 7.0 MeV clearly shows the effect of the total angular momentum (Le 64a), i.e., the first excited state (j = 1/2) angular distribution has a "dip" at about 100°, whereas no such "dip" occurs in the case of the ground state (j = 3/2). It should be mentioned that this "dip" associated with the first excited state has been observed experimentally at E_d = 7.0 MeV by Kashy et al. (Ka 64). Unfortunately, they do not give a listing of their experimental differential cross sections so that no direct comparison is possible. Note

Figure 4.9   Angular distributions of the ^{48}Ca(d,p)^{49}Ca(2.028)

reaction.

Figure 4.10   Angular distributions of the ^{48}Ca(d,p)^{49}Ca(2.028)

reaction

In both figures the lines are the DWBA predictions.

The solid and dashed lines refer to the proper

and average parameters respectively.

$^{48}Ca(d,p)^{49}Ca(2.028)$
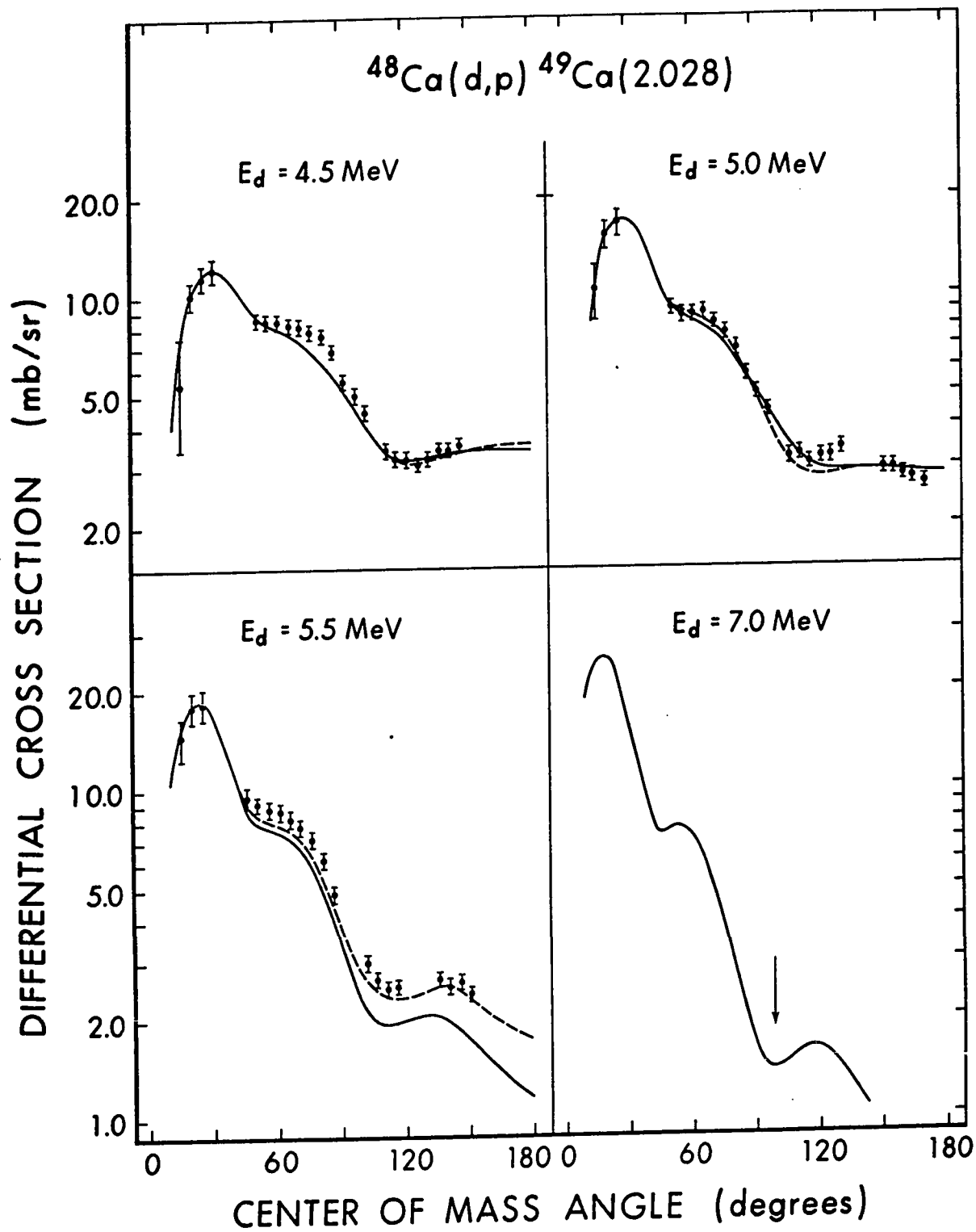
$^{48}Ca(d,p)$ $^{49}Ca(2.028)$

Figure 4.11   Yield curves of the ^{48}Ca(d,p)^{49}Ca(2.028) reaction. The solid lines are the DWBA predictions calculated from the average deuteron parameters.
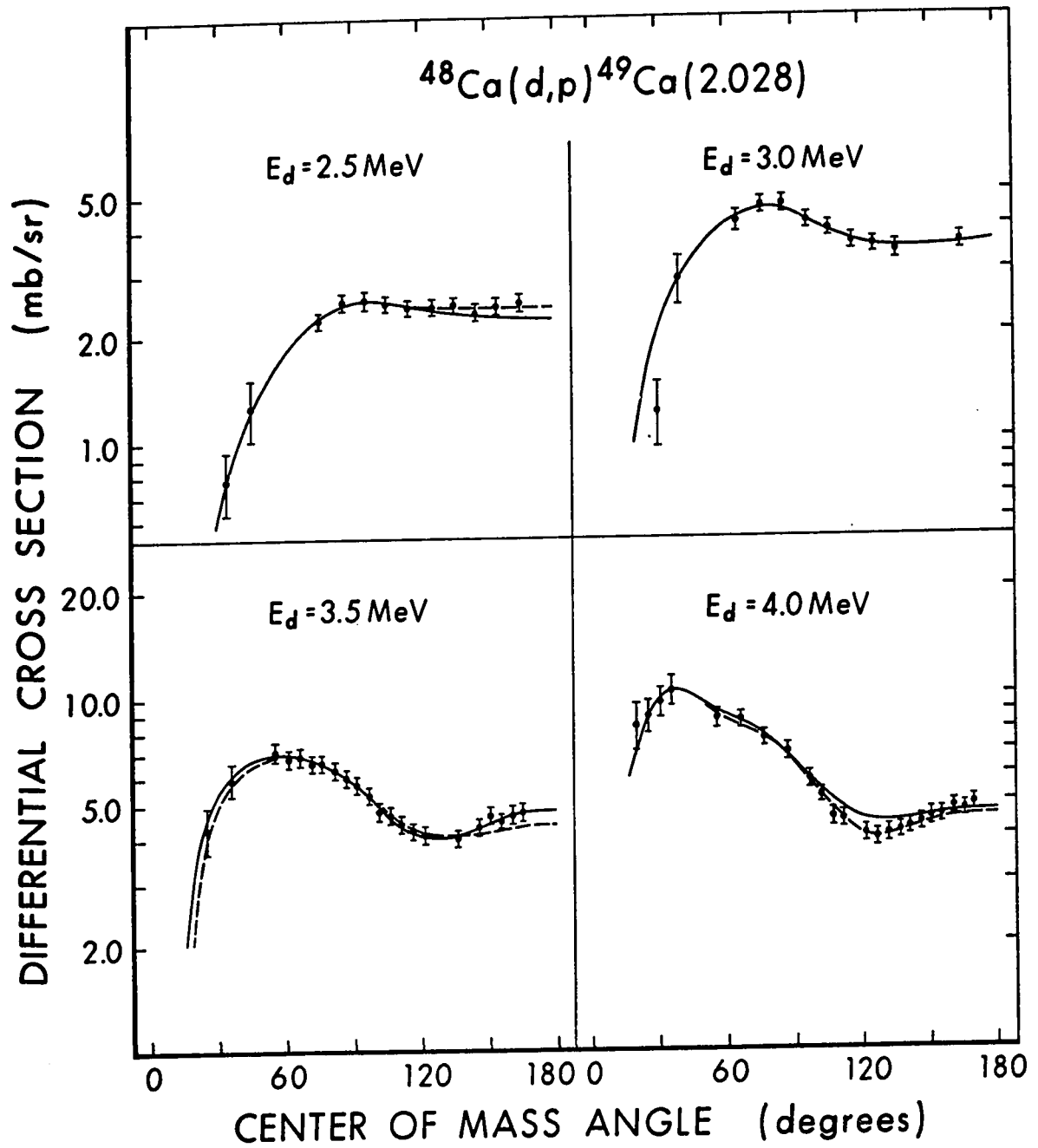
$^{48}Ca(d,p)$ $^{49}Ca(2.028)$

65°

90°

115°

145°

165°

DEUTERON ENERGY (MeV)

DIFFERENTIAL CROSS SECTION (mb/sr)
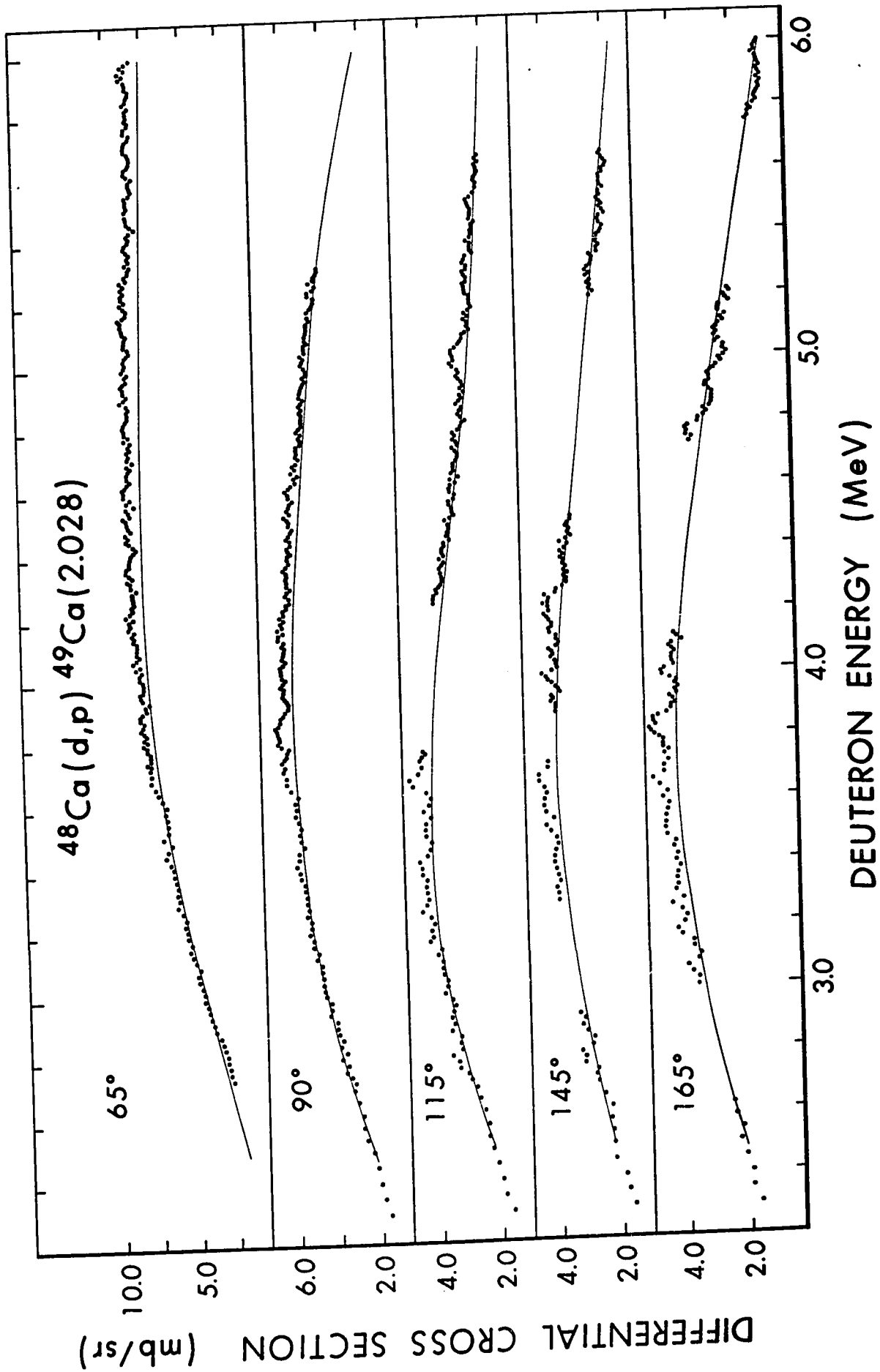
that even at E_d = 5.5 MeV the predicted angular distributions

exhibit the j-dependent behaviour to some extent.

The spectroscopic factor

$$S = \frac{d\sigma(\Theta)}{d\Omega}\bigg|_{exp} \; [\frac{d\sigma(\Theta)}{d\Omega}\bigg|_{calc}]^{-1}$$

was obtained from the previously mentioned normalization. A

listing of S for both states and both sets of deuteron parameters

is given in Table 4.3. This table is presented graphically in

Fig. 4.12, where the solid and open circles refer to the average

and proper parameters respectively. It is seen from Fig. 4.12

that the proper deuteron parameters produce a spectroscopic factor

that varies greatly with energy, whereas the average deuteron para-

meters produce a spectroscopic factor that is constant with energy.

Since the spectroscopic factor is a measure of the extent to which

a state is a single-particle state, it is independent of energy

and it is clear that average deuteron parameters must be used in

DWBA calculations. The energy-averaged spectroscopic factor

(only the spectroscopic factors obtained from the average deuteron

parameters were included) is 0.98 for the ground state and 1.06 for

the first excited state. The spectroscopic factors are close to

TABLE 4.3

SPECTROSCOPIC FACTORS

Deuteron Energy E_d	$^{48}Ca(d,p)^{49}Ca(0)$		$^{48}Ca\ (d,p)^{49}Ca(2.028)$	
	Proper d-Parameters	Average d-Parameters	Proper d-Parameters	Average d-Parameters
2.5	0.98	1.00	1.12	1.09
3.0	1.21	0.95	1.18	1.04
3.5	1.36	1.06	1.30	1.06
4.0	0.96	0.96	1.08	1.08
4.5	0.97	0.97	1.03	1.03
5.0	0.75	0.95	0.94	1.09
5.5	1.04	0.95	1.15	1.06
7.0		1.02		

Figure 4.12   The spectroscopic factors of the $^{48}Ca(d,p)^{49}Ca(0)$ and $^{48}Ca(d,p)^{49}Ca(2.028)$ reactions. The open and closed circles refer to the proper and average deuteron parameters respectively.
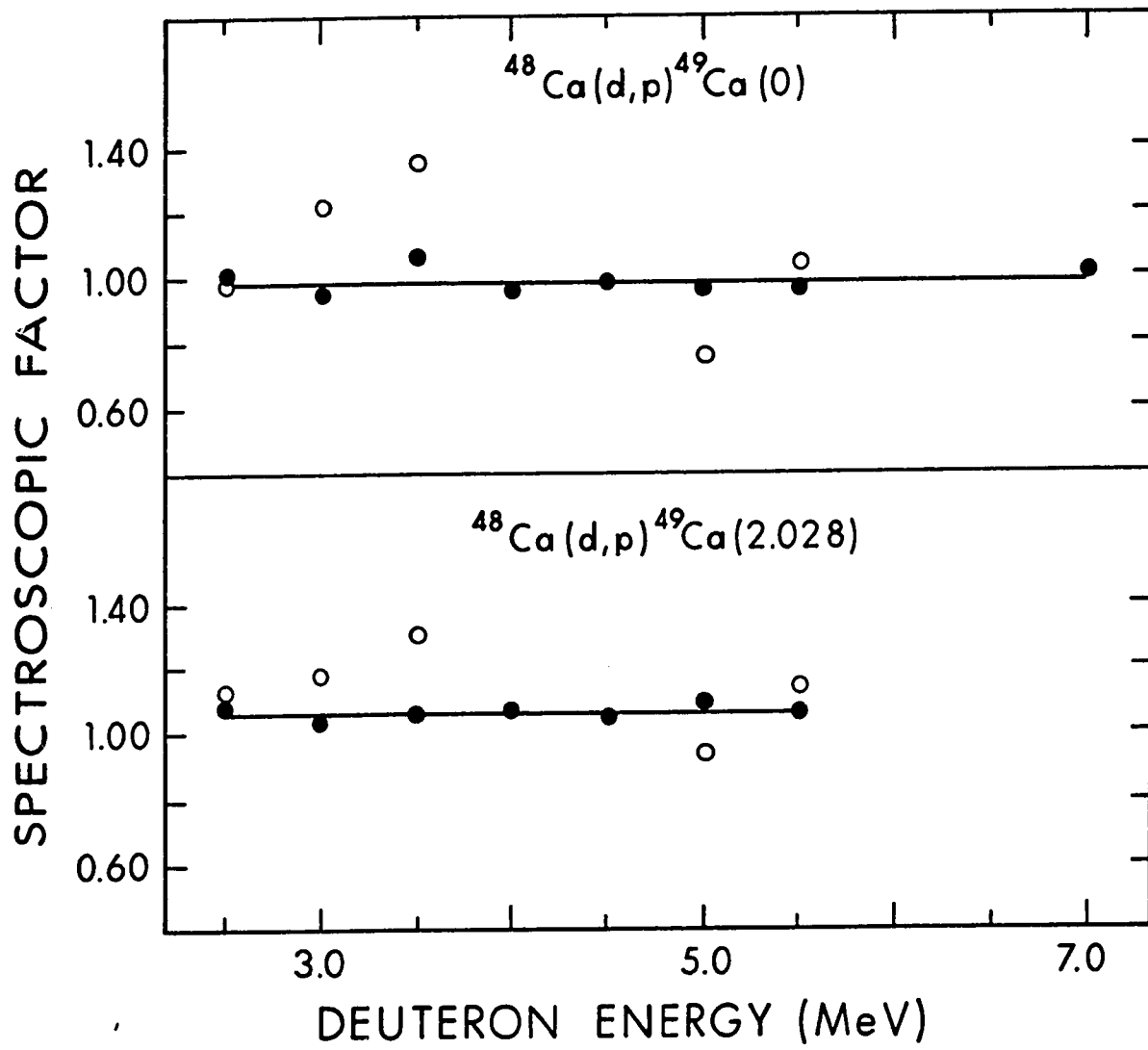
unity as anticipated, since the states in ^{49}Ca were expected

to be good single-particle states. A comparison of the

spectroscopic factors, calculated with the captured neutron

parameters as determined by Schiffer (Sc 69a), Becchetti and

Greenlees (Be 69), Rosen (Ro 66) and this study is shown in

Table 4.4. The spectroscopic factor has been estimated from

the previously stated relationships between the radius, the

diffuseness and the cross section.

The angular distributions of the vector analyzing power

of the ^{48}Ca(d,p)^{49}Ca(0) and ^{48}Ca(d,p)^{49}Ca(2.028) reactions are

shown in Fig. 4.13; the DWBA predictions are shown as solid

lines. The predicted analyzing power is calculated from the

deuteron vector polarization of the inverse reaction

^{49}Ca(p,d)^{48}Ca, since the analyzing power in a (d,p) reaction

is identical to the deuteron vector polarization in a (p,d)

reaction (Bl 52, Sa 58, Bi 59). It should be noted that

again the calculations reproduce the first excited state data

better than the ground state data.

It has been shown by Huby et al. (Hu 58) that if spin-

orbit potential effects are negligible, there exists a simple

relationship between the analyzing power P_d^r of two transitions

which have the same orbital angular momentum transfer and the

same excitation energy. This relationship is

TABLE 4.4

SPECTROSCOPIC FACTORS FOR VARIOUS NEUTRON PARAMETER SETS

Source	Neutron Parameters			Spectroscopic Factor	
	r(fm)	a(fm)	V_{SO}(MeV)	^{49}Ca(0)	^{49}Ca(2.028)
Present Work	1.15	0.65	8	0.98	1.06
Schiffer	1.07	0.65		1.19	1.28
Becchetti and Greenlees	1.17	0.75	6.2	0.78	0.85
Rosen	1.25	0.65	5.5	0.72	0.79

Figure 4.13   Angular distributions of the vector

analyzing power of the ^{48}Ca(d,p)^{49}Ca(0)

and ^{48}Ca(d,p)^{49}Ca(2.028) reactions.

The solid lines are the DWBA predictions.

$^{48}Ca\,(d,p)^{49}Ca\,(0)$

$^{48}Ca\,(d,p)^{49}Ca\,(2.028)$
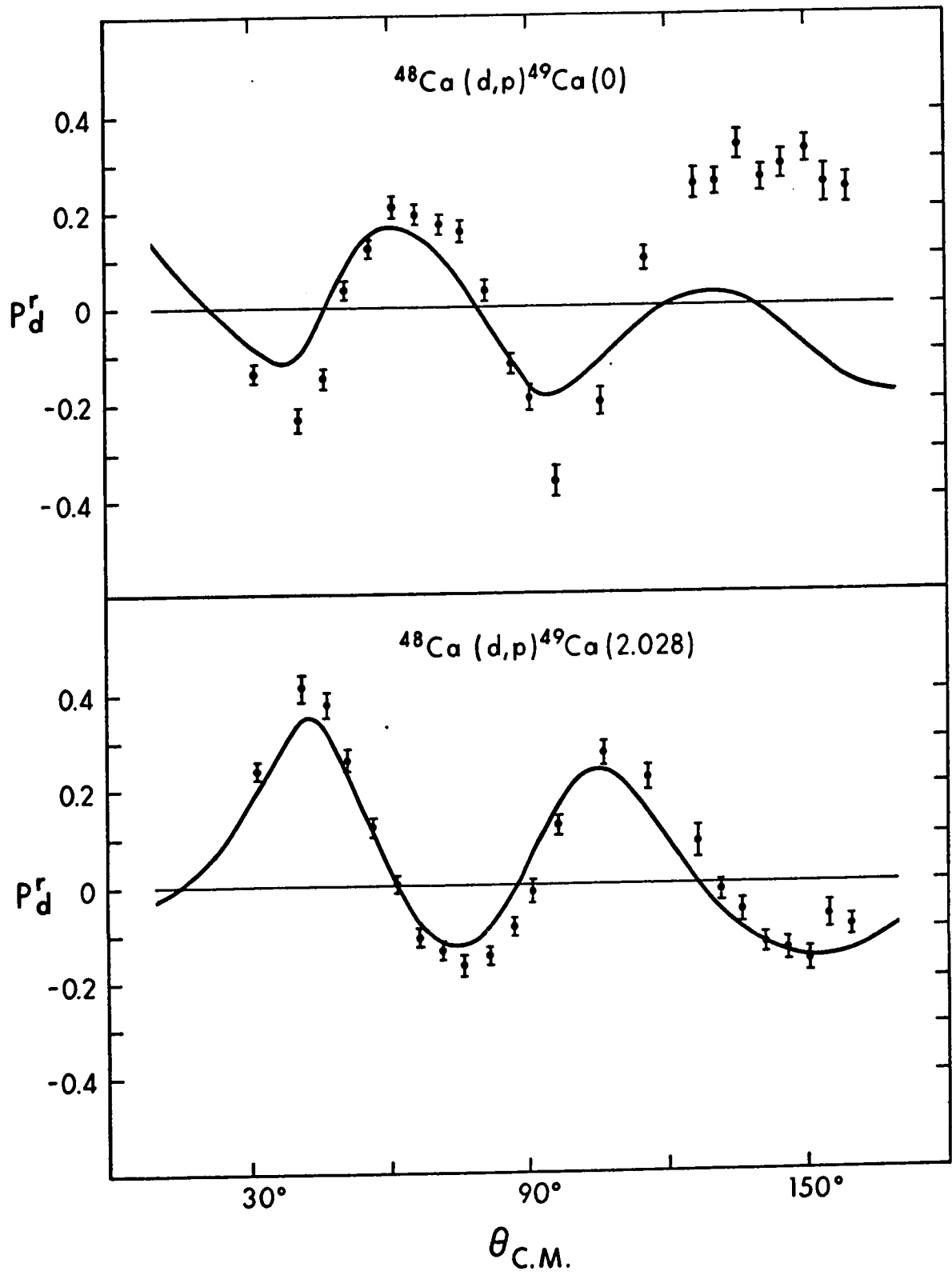
$$\frac{[P_d^r]_{j\,=\,\ell\,+\,1/2}}{[P_d^r]_{j\,=\,\ell\,-\,1/2}} = -\frac{\ell}{\ell+1}$$

i.e., P_d^r for different j states is exactly out of phase and

the magnitude of P_d^r is different by a factor $\ell/(\ell+1)$.

Yule and Haeberli (Yu 68) have shown that for intermediate

nuclei and low energies the spin-orbit effects are small.

Since both states under consideration are $\ell = 1$ states,

only the condition that the excitation energy be the same is

not fulfilled. It is therefore expected that the relationship

should hold approximately, and it is seen from Fig. 4.13 that

the angular distributions of the two states are almost exactly

out of phase and that the magnitude of P_d^r for the ground state

is approximately half the magnitude of P_d^r for the first excited

state at forward angles, in good agreement with theory. It

is therefore concluded that the ground state has spin $j = 3/2$

and that the first excited state has spin $j = 1/2$, in agreement,

with the previous assignment (Le 64a).

The remainder of this chapter will deal with some

aspects of the DWBA analysis that have not as yet been discussed.

In many cases the angular distributions of the elastically

scattered deuteron and the reaction proton (or neutron in the

(d,n) reaction) are not obtained simultaneously so that

absolute cross sections must be determined independently for

the two sets of data. Since this procedure may introduce a relative error in the deuteron and proton cross sections, it was felt that it was of some interest to determine to what extent such a relative error would affect the spectroscopic factor. The deuteron cross sections were therefore increased by 5% and the usual Optical Model analysis was applied. The resulting deuteron parameters were then used in a DWBA calculation and the results compared to a standard calculation. It was found that the shape of the predicted proton angular distribution was unchanged but the cross section was increased by 5%. It is clear, therefore, that such a relative error is strongly transmitted to the spectroscopic factor. By the same token, if the cross sections for both sets of data share a common error, which can occur if the sets of data are taken simultaneously, this error is not transmitted to the spectroscopic factor.

The imaginary well depth W is the only deuteron parameter that shows a definite and strong energy dependence according to the Optical Model analysis. In order to verify that this energy dependence was needed in the DWBA calculations, the dependence of the spectroscopic factor on W was determined. It was found that a decrease of 1.3 MeV in W caused an increase of 5% in the spectroscopic factor. Since $W \propto 1.3\ E_d(MeV)$, it is clear that this energy dependence is indeed needed to obtain a constant spectroscopic factor.

CHAPTER 5

SUMMARY AND CONCLUSIONS

The results and conclusions of the study presented in this thesis will be summarized in this chapter.

(1) Optical Model

The Optical Model analysis method originated in the course of this study is described below for the two cases that have been investigated.

a) Cross section data only

The spin-orbit parameters V_{SO}, r_{SO} and a_{SO} are fixed at acceptable values. A grid-search is performed over the cross section data in which V and a_i are gridded and r_o, a_o, W and r_i are searched simultaneously (a grid-search means that each grid step is followed by a search).

b) Cross section and polarization data

First the spin-orbit parameters are determined from a grid-search over the cross section data in which a_i, V_{SO}, r_{SO} and a_{SO} are gridded and r_o, a_o, W and r_i are searched simultaneously. The real well depth V is held fixed at about 100 MeV and the spin-orbit parameters are selected on the basis of a visual fit

to the polarization data. The procedure outlined

for case a) is then followed with these spin-orbit

parameters.

Two comments must be made regarding the results of this

analysis method:

(1) the central parameters and χ^2 vary smoothly over the

range of V that is gridded (for deuterons this range

is nominally from about 90 MeV to about 130 MeV). In

addition χ^2 is virtually constant over this range and

cannot determine the optimum real well depth so that

an external criterion (such as a DWBA calculation) is

needed for this determination.

(2) Because of the visual fit to the polarization data,

the spin-orbit parameters are only determined nominally.

The above method was developed from the following obser-

vations:

(1) that the fit to the polarization data is poor so that

the χ^2 for the polarization data cannot be used as a

criterion in a search routine and this data must be

fitted visually.

(2) that only four central parameters (r_o, a_o, W and r_i)

should be searched simultaneously.

(3) that a search of these central parameters over the

cross section data establishes the basically correct

shape for the polarization.

(4) that the spin-orbit parameters affect the fit to the
cross section data very little.

Deuteron parameters were determined with the above method
at seven energies between 2.5 MeV and 5.5 MeV. The parameters
are quite smooth over the energy range, as expected from the
smooth behaviour of the elastic scattering yield curve, and
average parameters for the energy range were determined. Only
the imaginary well depth shows an energy dependence. This
energy dependence is given by $W = (1.3\ E(MeV) + 3.3)$ MeV for
the range $E_d = 2.5 - 5.5$ MeV.

The Optical Model analysis clearly shows the central
parameter ambiguities but it is difficult to determine what
combination of parameters constitutes an ambiguity or what
correlations exist between the parameters. It would be of
interest to determine these correlations since as yet no
generalized set of deuteron parameters exists. For example,
the ^{40}Ca parameters, determined by Schwandt and Haeberli
(Sc 69) do not fit the ^{48}Ca elastic scattering.

The Optical Model is deficient in that it cannot fit
the deuteron polarization properly. However, the Optical Model
does show, on the basis of the combined cross section and
polarization data, that the real well depth for the deuteron
must be in the range of 90 MeV to 130 MeV, i.e., approximately
100 MeV, since parameter sets around 50 MeV or around 150 MeV
do not give acceptable fits to the cross section and polarization
data.

(2) <u>DWBA</u>

It is important that the (d,d) and (d,p) angular distributions be obtained simultaneously since a relative error in the cross sections of the two sets of data is strongly transmitted to the spectroscopic factor through the deuteron Optical Model parameters.

Although the shapes of the angular distributions predicted from the proper and average deuteron parameters are nearly the same, the cross sections differ widely and average deuteron parameters had to be used in order to obtain a constant spectroscopic factor over the energy range. Since even in this case, where the deuteron elastic scattering yield curve is very smooth, the proper deuteron parameters cannot generate a constant spectroscopic factor, it must be concluded that, in general, average deuteron parameters must be used in DWBA calculations.

The radius of the neutron well was determined from the requirement that the neutron real well depth be the same for both the ground and first excited state and that the spin-orbit potential account for the difference in the binding energy of the two states. Equal well depths of 54.4 MeV were obtained for a neutron well radius of 1.15 fm, with the diffuseness a = 0.65 fm and the spin-orbit well depth V_{SO} = 8 MeV.

The deuteron, proton and neutron parameters used in this study are listed below.

(deuteron parameters)

$V = 95.0$ MeV $\qquad W = (1.3 \ E(\text{MeV}) + 3.3)$ MeV $\qquad V_{SO} = 10.0$ MeV

$r_o = 1.17$ fm $\qquad r_i = 1.48$ fm $\qquad\qquad r_{SO} = 0.91$ fm

$a_o = 0.71$ fm $\qquad a_i = 0.66$ fm $\qquad\qquad a_{SO} = 0.60$ fm

(proton parameters)

$V = 51.4$ MeV $\qquad W = 8.6$ MeV $\qquad\qquad V_{SO} = 7.5$ MeV

$r_o = 1.24$ fm $\qquad r_i = 1.19$ fm $\qquad\qquad r_{SO} = 1.24$ fm

$a_o = 0.63$ fm $\qquad a_i = 0.64$ fm $\qquad\qquad a_{SO} = 0.63$ fm

(neutron parameters)

$$r_o = 1.15 \text{ fm}$$

$$a_o = 0.65 \text{ fm}$$

$$V_{SO} = 8 \text{ MeV}$$

The spectroscopic factor, obtained from the above parameters, is 0.98 ± 0.08 for the ground state and 1.06 ± 0.08 for the first excited state, where the error is the experimental error. These spectroscopic factors are close to unity, as anticipated, but it is to be noted that they are very sensitive to the neutron well radius and, to a lesser extent, the diffuseness. Thus, if neutron parameters determined by other authors are used, the spectroscopic factors are 20 - 30% higher or lower. It is suggested therefore that this method of determining neutron parameters be investigated in other nuclei.

The vector analyzing power of the (d,p) reactions was well reproduced by the DWBA calculations, particularly in the case of the first excited state, and the previous assignment of the j-values of the ground and first excited state, based on the empirical j-dependence of the cross section, was confirmed. It must be concluded, however, that although the spin-orbit parameters are needed to fit the polarization data, both the Optical Model and the DWBA theory show a rather low sensitivity to these parameters so that they can only be determined nominally.

Calculations at E_d = 7.0 MeV showed the characteristic "dip" for the j = 1/2 first excited state whereas no such dip occurred for the j = 3/2 ground state. It was therefore concluded that DWBA theory does reproduce the observed j-dependence of the angular distributions.

The DWBA calculations fit the forward angles of the ground state angular distributions well, except around the second stripping peak. The fit to the backward angles is poor, but this is to be expected, since the yield curves show large fluctuations at angles greater than 90°. It should be noted, however, that even at the backward angles, the overall shape of the ground state yield curve is well predicted by the DWBA calculations.

In the case of the first excited state the DWBA calculations reproduce the experimental angular distributions almost perfectly at all angles and over the entire energy

range, and the yield curves, which have quite small fluctuations, are remarkably well predicted by the DWBA calculations.

In view of the above findings, it is concluded that if fluctuations are small, and provided energy-averaged deuteron parameters are used, DWBA theory gives an excellent representation of the direct reaction process, above as well as below the Coulomb barrier and that reliable nuclear structure information can be extracted from both energy regions.

BIBLIOGRAPHY

An 68   S. A. Anderson and Ole Hansen and R. Chapman and
S. Hinds, Nucl. Phys. A120 (1968) 421

Ba 62   R. H. Bassel, R. M. Drisko and G. R. Satchler,
Oak Ridge National Laboratory Report ORNL-3240
(UC-34-Physics) 1962 (unpublished)

Be 65   T. A. Belote, A. Sperduto and W. W. Buechner,
Phys. Rev. 139 (1965) B80

Be 68   T. A. Belote, W. E. Dorenbusch and J. Rapaport,
Nucl. Phys. A120 (1968) 401

Be 69   F. D. Becchetti, Jr., and G. W. Greenlees, to be
published

Bi 59   L. C. Biedenharn, Nucl. Phys. 10 (1959) 620

Bj 58   F. Bjorklund and S. Fernbach, Phys. Rev. 109 (1958)
1295

Bl 52   R. Blin-Stoyle, Proc. Phys. Soc. A65 (1952) 452

Bl 55   R. J. Blin-Stoyle, Phil. Mag. 46 (1955) 973

Bl 62   John M. Blatt and Victor F. Weisskopf, Theoretical
Nuclear Physics (John Wiley & Sons, 1962)

Bu 64   P. J. A. Buttle and L. J. B. Goldfarb, Proc. Phys.
Soc. 83 (1964) 701

Cl 67   T. B. Clegg, G. R. Plattner, L. G. Keller and
W. Haeberli, Nucl. Instr. and Meth. 57 (1967) 167

Da 69   N. E. Davison, Ph.D. Thesis, University of Alberta
(1969)

Da 69a   N. E. Davison, University of Alberta, Nuclear
Research Centre Internal Report (1969) unpublished

Em 63   W. S. Emmerich, Fast Neutron Physics, Part II,
(Interscience Publishers, 1963)

Fi 68   W. Fitz, R. Jahr and R. Santo, Nucl. Phys. $\underline{A114}$
         (1968) 392

Gi 66   F. P. Gibson and A. K. Kerman, Phys. Rev. $\underline{145}$
         (1966) 758

Go 65   L. J. B. Goldfarb, Nucl. Phys. $\underline{72}$ (1965) 537

Gr 68   G. W. Greenlees, G. J. Pyle, and Y. C. Tang, Phys.
         Rev. $\underline{171}$ (1968) 1115

Ha 67   W. Haeberli, Annual Review of Nuclear Science $\underline{17}$
         (1967) 373

He 68   W. R. Hering and M. Dost, Nucl. Phys. $\underline{A111}$ (1968)
         561

Hj 65   S. A. Hjorth, J. X. Saladin and G. R. Satchler,
         Phys. Rev. $\underline{138}$ (1965) B1425

Hu 58   R. Huby, M. Y. Refai and G. R. Satchler, Nucl. Phys.
         $\underline{9}$ (1958) 94

Hu 69   R. G. Humphries, M.Sc. Thesis, University of Alberta
         (1969)

Ja 55   Z. Jankovic, Phil. Mag. $\underline{46}$ (1955) 376

Ka 64   E. Kashy, A. Sperduto, H. A. Enge and W. W. Buechner,
         Phys. Rev. $\underline{135}$ (1964) B865

Le 64   L. L. Lee, Jr., J. P. Schiffer and B Zeidman and
         G. R. Satchler, R. M. Drisko and R. M. Bassel,
         Phys. Rev. $\underline{136}$ (1964) B971

Le 64a   L. L. Lee and J. P. Schiffer, Phys. Rev. Letters $\underline{12}$
         (1964) 108

Le 68   H. G. Leighton, Ph.D. Thesis, University of Alberta
         (1968)

Ma 64   B. Macefield, Nucl. Phys. $\underline{59}$ (1964) 573

Ma 64a   B. Macefield and R. Middleton, Nucl. Phys. $\underline{59}$ (1964)
         561

Ma 66   A. Marinov, L. L. Lee, Jr., and J. P. Schiffer,
         Phys. Rev. $\underline{145}$ (1966) 852

Ne 55   . P. E. Nemirovski, Proc. Intern. Conf. Peaceful Uses Atomic Energy, Vol. II, Geneva, 1955

Ob 66   A. W. Obst, M.Sc. Thesis, University of Alberta (1966)

Pe 62   F. G. Perey and B. Buck, Nucl. Phys. $\underline{32}$ (1962) 353

Pe 63   F. G. Perey, Phys. Rev. $\underline{131}$ (1963) 745

Pe 67   F. G. Perey and G. R. Satchler, Nucl. Phys. $\underline{A97}$ (1967) 515

Ro 61   D. Robson, Nucl. Phys. $\underline{22}$ (1961) 47

Ro 66   L. Rosen, Proc. 2nd Int. Symp. on Polarization Phenomena of Nucleons, Karlsruhe, September 1965 (Birkhäuser Verlag, 1966)

Ro 69   G. Roy and N. Riebeck, Nucl. Instr. and Methods $\underline{71}$ (1969) 234

Sa 58   G. R. Satchler, Nucl. Phys. $\underline{8}$ (1958) 65

Sa 60   G. R. Satchler and W. Tobocman, Phys. Rev. $\underline{118}$ (1960) 1566

Sc 68   P. Schwandt and W. Haeberli, Nucl. Phys. $\underline{A110}$ (1968) 585

Sc 69   P. Schwandt and W. Haeberli, Nucl. Phys. $\underline{A123}$ (1969) 401

Sc 69a   J. P. Schiffer, Proc. of the Conf. on Nuclear Isospin, Asilomar – Pacific Grove (Academic Press, 1969)

Se 69   Kamal K. Seth, J. Picard, G. R. Satchler, to be published in Nuclear Physics

Sm 65   W. R. Smith, Oak Ridge National Laboratory Report ORNL-TM-1117 (1965) unpublished

To 61   W. Tobocman, Theory of Direct Nuclear Reactions, (Oxford University Press, 1961)

Ul 68   W. Ulrici and W. R. Hering, Nucl. Phys. $\underline{A110}$ (1968) 281

Vo 62   E. Vogt, Rev. Mod. Phys. $\underline{34}$ (1962) 723

Vo 68   E. Vogt, Advances in Nuclear Physics $\underline{1}$ (1968) 261

Wa 68   Bruce A. Watson, Informal Report PHY-1968B Argonne
         Physics Division

Yu 68   T. J. Yule and W. Haeberli, Nucl. Phys. $\underline{A117}$ (1968) 1

APPENDIX $\underline{B}$

Jo 66   K. W. Jones and J. P. Schiffer, L. L. Lee, A. Marinov
         and J. L. Learner, Phys. Rev. $\underline{145}$ (1966) 894.

Mo 66   C. Fred Moore, Charles E. Watson, S. A. A. Zaidi, James
         J. Kent, and James G. Kulleck, Phys. Rev. Letters $\underline{17}$
         (1966) 926.

Sh 68   J. F. Sharpey-Schafer, Phys. Letters $\underline{26B}$ (1968) 652.

APPENDIX A

TABLES OF DIFFERENTIAL CROSS SECTIONS AND ANALYZING POWER

In this appendix the differential cross sections and
the analyzing power for the angular distributions are listed.
The ^{48}Ca(d,d)^{48}Ca differential cross sections have an
experimental error of 2.5% for angles of 65° and greater; for
angles smaller than 65° the error is 5%. The ^{48}Ca(d,p)^{49}Ca(0)
and ^{48}Ca(d,p)^{49}Ca(2.028) differential cross sections have an
experimental error of 5%, except at forward angles where the
percentage error is indicated by the figure in brackets. The
error listed for the analyzing power is purely statistical.

The overall error in the differential cross sections
is estimated to be less than 8%.

$$^{48}Ca(d,d)^{48}Ca$$

Lab. Angle (degrees)	C.M. Angle (degrees)	E_d = 2.5 MeV	E_d = 3.0 MeV
		$\frac{d\sigma}{d\Omega}_{C.M.}$ (mb/sr)	$\frac{d\sigma}{d\Omega}_{C.M.}$ (mb/sr)
55.0	57.0	1820	
60.0	62.1		899
65.0	67.2	962	633
75.0	77.3	579	376
85.0	87.4	384	247
95.0	97.4	273	175
105.0	107.3	205	132
115.0	117.2	161	107
125.0	127.0	133	88.0
135.0	136.7	114	76.8
145.0	146.4	.101	68.3
155.0	156.0	93.8	62.9
165.0	165.6	88.2	58.2

^{48}Ca(d,d)^{48}Ca

Lab. Angle (degrees)	C.M. Angle (degrees)	E_d = 3.5 MeV	E_d = 4.0 MeV
		$\frac{d\sigma}{d\Omega}_{C.M.}$ (mb/sr)	$\frac{d\sigma}{d\Omega}_{C.M.}$ (mb/sr)
45.0	46.7		1330
50.0	51.9		852
55.0	57.0	837	583
65.0	67.2	430	298
70.0	72.3	312	
75.0	77.3	243	166
80.0	82.4	193	
85.0	87.4	157	108
90.0	92.4	130	
95.0	97.4	114	78.8
100.0	102.4	98.7	70.1
105.0	107.3	87.4	62.2
110.0	112.3	78.9	56.2
115.0	117.2	71.8	50.9
120.0	122.1	65.2	46.8
125.0	127.0	60.3	42.2
130.0	131.9	56.2	37.9
135.0	136.7	51.7	34.3
140.0	141.6	47.7	31.4
145.0	146.4	44.8	29.2
150.0	151.2	43.1	27.1
155.0	156.0	41.0	25.1
160.0	160.8	38.5	24.1
165.0	165.6	37.4	22.8
170.0	170.4		22.6

$$^{48}Ca(d,d)^{48}Ca$$
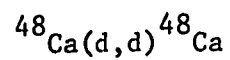
Lab. Angle (degrees)	C.M. Angle (degrees)	E_d = 4.5 MeV $\frac{d\sigma}{d\Omega}_{C.M.}$ (mb/sr)	E_d = 5.0 MeV $\frac{d\sigma}{d\Omega}_{C.M.}$ (mb/sr)
40.0	41.6	1520	1180
45.0	46.7	963	722
50.0	51.9	615	460
55.0	57.0	416	303
60.0	62.1	291	214
65.0	67.2	205	152
70.0	72.3	150	112
75.0	77.3	112	83.2
80.0	82.4	90.7	67.3
85.0	87.4	75.4	56.6
90.0	92.4	64.8	48.6
95.0	97.4	56.4	42.6
100.0	102.4	51.0	37.7
105.0	107.3	44.9	33.6
110.0	112.3	41.4	29.8
115.0	117.2	37.0	26.5
120.0	122.1	32.6	22.6
125.0	127.0	28.4	19.8
130.0	131.9	25.6	16.8
135.0	136.7	22.8	15.1
140.0	141.6	20.5	13.5
145.0	146.4	18.0	11.9
150.0	151.2	16.5	11.1
155.0	156.0	15.7	10.6
160.0	160.8	14.5	10.1
165.0	165.6	14.0	9.64
170.0	170.4	13.7	9.72

^{48}Ca(d,d)^{48}Ca
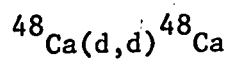
Lab. Angle (degrees)	C.M. Angle (degrees)	E_d = 5.5 MeV $\frac{d\sigma}{d\Omega}_{C.M.}$ (mb/sr)
40.0	41.6	940
45.0	46.7	568
50.0	51.9	361
55.0	57.0	240
60.0	62.1	162
65.0	67.2	113
70.0	72.3	83.3
75.0	77.3	62.7
80.0	82.4	51.2
85.0	87.4	42.5
90.0	92.4	36.5
95.0	97.4	32.7
100.0	102.4	29.2
105.0	107.3	26.3
110.0	112.3	23.2
115.0	117.2	20.1
120.0	122.1	17.1
125.0	127.0	14.7
130.0	131.9	12.7
135.0	136.7	11.1
140.0	141.6	10.2
145.0	146.4	9.56
165.0	165.6	9.14
170.0	170.4	9.46

$$^{48}\text{Ca}(d,p)^{49}\text{Ca}(0)$$

Lab. Angle (degrees)	C.M. Angle (degrees)	E_d = 2.5 MeV $\frac{d\sigma}{d\Omega}_{\text{C.M.}}$ (mb/sr)	E_d = 3.0 MeV $\frac{d\sigma}{d\Omega}_{\text{C.M.}}$ (mb/sr)
30.0	30.6		1.99 (15)
35.0	35.7	1.09 (10)	
40.0	40.8		3.12 (10)
45.0	45.9	1.21 (10)	
50.0	51.0		3.47
55.0	56.1	1.56	
60.0	61.1		3.96
65.0	66.2	1.67	3.86
75.0	76.2	1.68	3.55
85.0	86.3	1.58	2.84
95.0	96.3	1.44	2.21
105.0	106.2	1.29	1.89
115.0	116.2	1.28	1.83
125.0	126.1	1.16	1.92
135.0	135.9	1.20	2.09
145.0	145.7	1.07	2.25
155.0	155.5	1.14	2.25
165.0	165.3	1.14	2.24

$$^{48}\text{Ca}(d,p)^{49}\text{Ca}(0)$$

Lab. Angle (degrees)	C.M. Angle (degrees)	$E_d = 3.5$ MeV $\frac{d\sigma}{d\Omega}_{C.M.}$ (mb/sr)		$E_d = 4.0$ MeV $\frac{d\sigma}{d\Omega}_{C.M.}$ (mb/sr)	
20.0	20.4			8.85	(10)
25.0	25.5	5.15	(10)	10.8	(10)
30.0	30.6			10.2	
35.0	35.7	5.60		9.70	
40.0	40.8	5.66		9.10	
45.0	45.9	5.69		8.04	
50.0	51.0	5.48		7.46	
55.0	56.1	5.85		7.02	
60.0	61.1	5.67			
65.0	66.2	5.89		7.49	
70.0	71.2	5.77			
75.0	76.2	5.68		7.07	
80.0	81.3	5.16			
85.0	86.3	4.68		5.66	
90.0	91.3	4.20			
95.0	96.3	3.60		4.19	
100.0	101.3	3.00		3.46	
105.0	106.2	2.79		3.08	
110.0	111.2	2.50		2.59	
115.0	116.2	2.23		2.47	
120.0	121.1	2.10		2.44	
125.0	126.1	2.07		2.35	
130.0	131.0	2.12		2.39	
135.0	135.9	2.09		2.29	
140.0	140.8	2.18		2.43	
145.0	145.7	2.16		2.53	
150.0	150.6	2.20		2.56	
155.0	155.5	2.20		2.63	
160.0	160.4	2.19		2.62	
165.0	165.3	2.20		2.62	
170.0	170.2			2.67	

$$^{48}\text{Ca}(d,p)^{49}\text{Ca}(0)$$
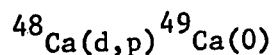
Lab. Angle (degrees)	C.M. Angle (degrees)	E_d = 4.5 MeV	E_d = 5.00 MeV
		$\dfrac{d\sigma}{d\Omega}_{\text{C.M.}}$ (mb/sr)	$\dfrac{d\sigma}{d\Omega}_{\text{C.M.}}$ (mb/sr)
15.0	15.3	7.73 (10)	12.8 (10)
20.0	20.4	13.7 (10)	17.9
25.0	25.5	15.9	19.2
30.0	30.6	14.4	16.6
35.0	35.7	12.7	13.1
40.0	40.8	10.1	10.8
45.0	45.9	8.90	9.46
50.0	51.0	8.28	8.68
55.0	56.1	8.12	9.42
60.0	61.1	8.10	8.98
65.0	66.2	8.09	8.82
70.0	71.2	7.98	7.81
75.0	76.2	6.65	7.10
80.0	81.3	6.04	5.52
85.0	86.3	4.92	4.32
90.0	91.3	3.94	3.30
95.0	96.3	3.02	2.71
100.0	101.3	2.40	2.23
105.0	106.2	1.86	2.04
110.0	111.2	1.77	2.09
115.0	116.2	1.59	2.25
120.0	121.1	1.61	2.24
125.0	126.1	1.73	2.28
130.0	131.0	1.78	2.38
135.0	135.9	1.97	2.23
140.0	140.8	2.06	2.31
145.0	145.7	2.05	2.15
150.0	150.6	2.06	2.01
155.0	155.5	2.13	1.82
160.0	160.4	2.13	1.54
165.0	165.3	2.13	1.30
170.0	170.2	2.07	1.07

^{48}Ca(d,p)^{49}Ca(0)
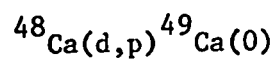
Lab. Angle (degrees)	C.M. Angle (degrees)	E_d = 5.5 MeV
		$\frac{d\sigma}{d\Omega}_{C.M.}$ (mb/sr)
15.0	15.3	17.4 (10)
20.0	20.4	22.7
25.0	25.5	21.9
30.0	30.6	17.7
35.0	35.7	13.3
40.0	40.8	9.44
45.0	45.9	8.13
50.0	51.0	8.20
55.0	56.1	9.22
60.0	61.1	9.42
65.0	66.2	9.03
70.0	71.2	8.44
75.0	76.2	6.70
80.0	81.3	5.27
85.0	86.3	3.83
90.0	91.3	2.95
95.0	96.3	2.35
100.0	101.3	2.16
105.0	106.2	2.04
110.0	111.2	2.23
115.0	116.2	2.33
120.0	121.1	2.53
125.0	126.1	2.57
130.0	131.0	2.70
135.0	135.9	2.56
140.0	140.8	2.48
145.0	145.7	2.32
150.0	150.6	2.22
155.0	155.5	2.23
160.0	160.4	1.93
165.0	165.3	1.81
170.0	170.2	1.57

$$^{48}CA(d,p)^{49}Ca(2.028)$$

Lab. Angle (degrees)	C.M. Angle (degrees)	E_d = 2.5 MeV $\frac{d\sigma}{d\Omega}_{C.M.}$ (mb/sr)	E_d = 3.0 MeV $\frac{d\sigma}{d\Omega}_{C.M.}$ (mb/sr)
30.0	30.8		1.20 (20)
35.0	35.9	0.78 (20)	
40.0	41.0		2.85 (15)
45.0	46.1	1.26 (20)	
65.0	66.4		4.12
75.0	76.5	2.21	4.54
85.0	86.5	2.48	4.56
95.0	96.5	2.52	4.10
105.0	106.5	2.46	3.87
115.0	116.4	2.40	3.62
125.0	126.3	2.42	3.49
135.0	136.1	2.43	3.37
145.0	145.9	2.31	
155.0	155.6	2.41	
165.0	165.4	2.47	3.61

$$^{48}\text{Ca}(d,p)^{49}\text{Ca}(2.028)$$

Lab. Angle (degrees)	C.M. Angle (degrees)	E_d = 3.5 MeV $\frac{d\sigma}{d\Omega}_{C.M.}$ (mb/sr)		E_d = 4.0 MeV $\frac{d\sigma}{d\Omega}_{C.M.}$ (mb/sr)	
20.0	20.5			8.23	(10)
25.0	25.6	4.23	(15)	8.70	(10)
30.0	30.8			9.47	(10)
35.0	35.9	5.93	(10)	10.3	(10)
55.0	56.3	7.07		8.51	
60.0	61.3	6.72			
65.0	66.4	6.77		8.51	
70.0	71.4	6.52			
75.0	76.5	6.51		7.52	
80.0	81.5	6.22			
85.0	86.5	5.90		6.79	
90.0	91.5	5.64			
95.0	96.5	5.24		5.75	
100.0	101.5	4.70		5.14	
105.0	106.5	4.61		4.45	
110.0	111.4	4.36		4.39	
115.0	116.4	4.22			
120.0	121.3	4.05		3.95	
125.0	126.3			3.91	
130.0	131.2			4.05	
135.0	136.1	3.95		4.11	
140.0	141.0			4.22	
145.0	145.9	4.27		4.33	
150.0	150.8	4.60		4.47	
155.0	155.6	4.38		4.53	
160.0	160.5	4.63		4.80	
165.0	165.4	4.67		4.64	
170.0	170.3			4.84	

$$^{48}\text{Ca}(d,p)^{49}\text{Ca}(2.028)$$

Lab. Angle (degrees)	C.M. Angle (degrees)	$E_d = 4.5$ MeV $\frac{d\sigma}{d\Omega}_{C.M.}$ (mb/sr)		$E_d = 5.0$ MeV $\frac{d\sigma}{d\Omega}_{C.M.}$ (mb/sr)	
15.0	15.4	5.44	(20)	10.5	(20)
20.0	20.5	10.2	(10)	15.4	(10)
25.0	25.6	11.5	(10)	16.6	(10)
30.0	30.8	12.2	(10)		
50.0	51.2	8.55		9.18	
55.0	56.3	8.53		8.72	
60.0	61.3	8.44		8.79	
65.0	66.4	8.21		8.92	
70.0	71.4	8.15		8.41	
75.0	76.5	7.79		7.75	
80.0	81.5	7.59		7.00	
85.0	86.5	6.84		5.78	
90.0	91.5	5.59		5.08	
95.0	96.5	5.02		4.50	
100.0	101.5	4.45			
105.0	106.5			3.26	
110.0	111.4	3.44		3.32	
115.0	116.4	3.25		3.11	
120.0	121.3	3.20		3.26	
125.0	126.3	3.11		3.25	
130.0	131.2	3.27		3.47	
135.0	136.1	3.42			
140.0	141.0	3.41			
145.0	145.9	3.56			
150.0	150.8			2.96	
155.0	155.6			3.01	
160.0	160.5			2.86	
165.0	165.4			2.77	
170.0	170.3			2.69	

$$^{48}Ca(d,p)^{49}Ca(2.028)$$
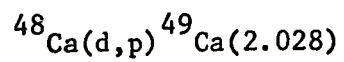
Lab. Angle (degrees)	C.M. Angle (degrees)	E_d = 5.5 MeV $\frac{d\sigma}{d\Omega}_{C.M.}$ (mb/sr)	
15.0	15.4	14.5	(15)
20.0	20.5	17.9	(10)
25.0	25.6	18.3	(10)
45.0	46.1	9.64	
50.0	51.2	9.08	
55.0	56.3	8.77	
60.0	61.3	8.63	
65.0	66.4	8.24	
70.0	71.4	7.75	
75.0	76.5	7.09	
80.0	81.5	6.17	
85.0	86.5	4.88	
100.0	101.5	2.99	
105.0	106.5	2.67	
110.0	111.4	2.51	
115.0	116.4	2.55	
135.0	136.1	2.68	
140.0	141.0	2.56	
145.0	145.9	2.61	
150.0	150.8	2.40	

^{48}Ca(d,d)^{48}Ca
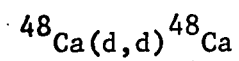
Lab. Angle (degrees)	C.M. Angle (degrees)	E_d = 5.5 MeV	
		P_d	
30.7	31.9	0.001	±0.001
40.3	41.8	0.013	±0.002
45.6	47.3	0.012	±0.002
50.1	52.0	0.003	±0.002
55.2	57.2	−0.002	±0.002
60.1	62.2	0.006	±0.003
65.1	67.3	·0.023	±0.003.
70.1	72.4	0.065	±0.005
74.7	77.0	0.111	±0.009
80.0	82.4	0.144	±0.010
85.4	87.8	0.166	±0.011
90.0	92.4	0.139	±0.010
95.0	97.4	0.095	±0.008
100.0	102.4	0.032	±0.009
104.9	107.3	−0.013	±0.007
109.9	112.2	−0.060	±0.010
114.5	116.7	−0.096	±0.010
119.5	121.6	−0.103	±0.015
125.2	127.2	−0.022	±0.013
130.2	132.1	0.005	±0.009
134.8	136.5	0.070	±0.011
139.8	141.3	0.150	±0.013
144.7	146.1	0.222	±0.017
149.6	150.8	0.305	±0.021
154.2	155.2	0.328	±0.025
159.1	159.9	0.321	±0.022

$^{48}Ca(d,p)^{49}Ca(0)$
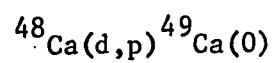
Lab. Angle (degrees)	C.M. Angle (degrees)	E_d = 5.5 MeV	
		P_d^r	
30.7	31.4	−0.139	±0.015
40.3	41.1	−0.236	±0.020
45.6	46.5	−0.149	±0.019
50.1	51.2	0.036	±0.015
55.2	56.3	0.120	±0.015
60.1	61.3	0.203	±0.020
65.1	66.3	0.190	±0.018
70.1	71.4	0.171	±0.017
74.7	76.0	0.154	±0.020
80.0	81.3	0.031	±0.017
85.4	86.8	−0.117	±0.020
89.6	91.0	−0.192	±0.029
95.0	96.4	−0.366	±0.030
104.9	106.2	−0.199	±0.024
114.5	115.8	0.094	±0.025
125.2	126.4	0.251	±0.032
130.2	131.3	0.254	±0.025
134.8	135.8	0.331	±0.030
139.8	140.7	0.261	±0.023
144.7	145.5	0.292	±0.030
149.6	150.3	0.223	±0.023
154.2	154.8	0.251	±0.036
159.1	159.5	0.237	±0.028

$$^{48}Ca(d,p)^{49}Ca(2.028)$$
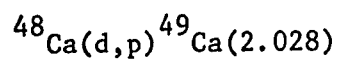
Lab. Angle (degrees)	C.M. Angle (degrees)	E_d = 5.5 MeV P_d^r	
30.7	31.5	0.238	±0.017
40.3	41.3	0.410	±0.025
45.6	46.7	0.374	±0.025
50.1	51.3	0.260	±0.020
55.2	56.5	0.121	±0.014
60.1	61.5	0.000	±0.015
65.1	66.5	−0.110	±0.013
70.1	71.6	−0.136	±0.014
74.7	76.2	−0.170	±0.018
80.0	81.5	−0.149	±0.016
85.4	87.0	−0.092	±0.016
89.6	91.2	−0.016	±0.022
95.0	96.6	0.121	±0.017
104.9	106.4	0.272	±0.023
114.5	116.0	0.220	±0.025
125.2	126.5	0.084	±0.027
130.2	131.4	−0.017	±0.017
134.8	135.9	−0.062	±0.021
139.8	140.8	−0.125	±0.016
144.7	145.6	−0.137	±0.024
149.6	150.4	−0.166	±0.017
154.2	154.9	−0.068	±0.028
159.1	159.6	−0.091	±0.021

APPENDIX B

Yield Curves

The yield curves, particularly those of the ground state, show significant fluctuations which are outside the statistical errors. These fluctuations may arise from a variety of sources: compound nucleus, analogue resonances, threshold effects, etc. The compound nucleus fluctuations are expected to be very narrow, 6 - 9 KeV, on the basis of Hauser-Feshbach calculations. Thus, in order to perform a fluctuation analysis, the energy steps in the yield curve should be of the order of 3 - 4 KeV, whereas in this case the steps were 10 KeV.

At the present time, no satisfactory explanation can be given for most of the wider fluctuations in the yield curves, but it appears that the sharp dip at $E_d = 4.27$ MeV in the ground state yield curve at 165° may be considered as an effect of the (d,n) and (d,p) coupling. This consideration is based on the fact that the coupling effect would be seen at a deuteron energy $E_p^{res} + B_d$, where E_p^{res} is the proton elastic scattering resonance energy for the analogue state of $^{49}Ca(0)$ in ^{49}Sc and B_d is the deuteron binding energy (Mo 66). Since $E_p^{res} = 1.96$ MeV (Jo 66) and $B_d = 2.22$ MeV, the coupling effect should be observed at $E_d = 4.18$ MeV, which is close to the observed dip in the yield curve.

Captured Neutron Parameters

In a recent paper, Sharpey-Schafer (Sh 68) has used the reformulated Optical Model of Greenlees, Pyle and Tang (Gr 68) to determine the captured neutron parameters. In this model the following relation exists:

$$7\pi^2 a_n^2 = 5<r^2>_R - 3r_n^2 A^{1/3} \qquad\qquad B.1$$

where a_n is the neutron well diffuseness

r_n is the neutron well radius

$<r^2>_R$ is the mean square radius of the real part of the Optical Model potential determined from elastic scattering (which can be determined to ± 4% (Sh 68)).

Since the mean square radius of ^{58}Ni is 3.92 ± 0.07 fm (Gr 68), it is found that the mean square radius of ^{48}Ca is 3.70 ± 0.07 fm if an $A^{1/3}$ dependence of $<r^2>_R^{1/2}$ is assumed.

The mean square radius determined from Eq. B.1 with the parameters determined in this thesis (r_n = 1.15 fm, a_n = 0.65 fm) is 3.75 fm. Thus the results of the reformulated Optical Model and the present determination agree within the quoted error.